Neurobiology of Aging 39 (2016) 1–18

Contents lists available at ScienceDirect

Neurobiology of Aging

journal homepage: www.elsevier.com/locate/neuaging

Mislocalization of neuronal tau in the absence of tangle pathology in phosphomutant tau knockin mice

Jonathan Gilley [a,*], Kunie Ando [b], Anjan Seereeram [c], Teresa Rodríguez-Martín [c], Amy M. Pooler [c], Laura Sturdee [a], Brian H. Anderton [c], Jean-Pierre Brion [b], Diane P. Hanger [c], Michael P. Coleman [a,1]

[a] Signalling Programme, The Babraham Institute, Cambridge, UK
[b] Laboratory of Histology, Neuroanatomy and Neuropathology, Faculty of Medicine, ULB Neuroscience Institute, Université Libre de Bruxelles, Brussells, Belgium
[c] Department of Basic and Clinical Neuroscience (PO37), Institute of Psychiatry, Psychology & Neuroscience, King's College London, London, UK

ARTICLE INFO

Article history:
Received 24 June 2015
Received in revised form 25 November 2015
Accepted 28 November 2015
Available online 7 December 2015

Keywords:
Tau
Knockin mouse
Hyperphosphorylation
Phosphomimetic
Phosphodefective
Tauopathy

ABSTRACT

Hyperphosphorylation and fibrillar aggregation of the microtubule-associated protein tau are key features of Alzheimer's disease and other tauopathies. To investigate the involvement of tau phosphorylation in the pathological process, we generated a pair of complementary phosphomutant tau knockin mouse lines. One exclusively expresses phosphomimetic tau with 18 glutamate substitutions at serine and/or threonine residues in the proline-rich and first microtubule-binding domains to model hyperphosphorylation, whereas its phosphodefective counterpart has matched alanine substitutions. Consistent with expected effects of genuine phosphorylation, association of the phosphomimetic tau with microtubules and neuronal membranes is severely disrupted in vivo, whereas the phosphodefective mutations have more limited or no effect. Surprisingly, however, age-related mislocalization of tau is evident in both lines, although redistribution appears more widespread and more pronounced in the phosphomimetic tau knockin. Despite these changes, we found no biochemical or immunohistological evidence of pathological tau aggregation in mice of either line up to at least 2 years of age. These findings raise important questions about the role of tau phosphorylation in driving pathology in human tauopathies.

1. Introduction

Neurodegenerative disorders termed tauopathies are characterized by aggregation of microtubule-associated protein tau into neurofibrillary tangles (NFTs). Among these, Alzheimer's disease (AD) is the most common, but mutations in the *MAPT* gene encoding tau have yet to be implicated as a causative factor. Instead, *MAPT* mutations are associated with a familial tauopathy, frontotemporal dementia with parkinsonism linked to tau mutations on chromosome 17 (FTDP-17T), which is an early-onset, autosomal-dominant disorder (Wolfe, 2009). Although there is currently no clear unifying mechanism to encompass the effects of all the different FTDP-17T mutations, which include disruption of tau microtubule binding and alterations in the proportion of tau isoforms with 3 or 4 microtubule-binding domain (MTBD) repeats (3R or 4R tau), ultimately they all promote the formation of somatodendritic NFTs.

Tau is a phosphoprotein and over 40 serine, threonine, and tyrosine residues have been identified as sites of physiological or disease-associated phosphorylation (Hanger et al., 2009). Although a variety of kinases have the potential to phosphorylate these sites, the number of true in vivo tau kinases is probably more limited (Hanger et al., 2009). Phosphorylation of tau is less extensive in adult brain than fetal brain, but tau does become relatively hyperphosphorylated in NFTs and this occurs at many of the same sites that are phosphorylated during early development (Brion et al., 1993; Johnson and Stoothoff, 2004). However, because developmental phosphorylation of tau does not promote filamentous aggregation, the precise relationship of tau hyperphosphorylation to the pathological process leading to tauopathy remains unclear.

Many mouse models have been created to investigate the role of tau dysfunction in neurodegeneration, but the majority involve transgenic expression of nonphysiological levels of wild-type

* Corresponding author at: Signalling Programme, The Babraham Institute, Babraham Research Campus, Cambridge, CB22 3AT, UK. Tel.: +44 122 349 6634.
E-mail address: jon.gilley@babraham.ac.uk (J. Gilley).
[1] Present address: John van Geest Centre for Brain Repair, Robinson Way, Cambridge, UK.

0197-4580/
http://dx.doi.org/10.1016/j.neurobiolaging.2015.11.028

human tau isoforms or human tau isoforms bearing FTDP-17T mutations in the presence of endogenous murine tau (Denk and Wade-Martins, 2009; Noble et al., 2010). Although tau phosphorylation is often increased in these mice, assessing its impact separately from the effects of disease mutations, increased expression, and/or altered tau isoform ratios is not possible. Overexpression or activation of known tau kinases, such as glycogen synthase kinase-3β and cyclin-dependent kinase 5, increases tau phosphorylation and can also enhance somatodendritic aggregation of endogenous murine tau or transgene-expressed wild-type or mutant human tau in mice (Ahlijanian et al., 2000; Cruz et al., 2003; Noble et al., 2003; Spittaels et al., 2000; Terwel et al., 2008); however, these kinases are relatively promiscuous meaning that any experimental outcome cannot be conclusively attributed to specific tau phosphorylation sites, or even to their effects on tau alone.

More recently, transgenic mice expressing a permanently pseudohyperphosphorylated phosphomimetic human tau mutant, referred to as PHP tau, were generated to address the role of tau hyperphosphorylation more directly (Hundelt et al., 2011). Surprisingly, expression of PHP tau did not promote significant tau aggregation, NFT formation, or neurodegeneration in these mice, but this could have been due to a relatively low level of PHP tau expression and/or the unexpectedly limited effect that specific subset of modified sites appeared to have on normal tau function.

Here, we have generated two novel, complementary knockin mouse lines to investigate further the impact of phosphorylation of tau at multiple sites on both its normal physiological function and its potential role in driving pathological change. One exclusively expresses a stably pseudohyperphosphorylated tau mutant in which 18 phosphomimetic negative charges have been introduced at specific sites via glutamate substitutions, whereas its counterpart exclusively expresses phosphodefective tau in which incorporation of alanines at the same sites prevents phosphorylation. Comparison between the two should allow us to distinguish potentially phosphorylation-dependent effects from unrelated structural effects of the mutations. Sixteen of the modifications are concentrated in the proline-rich domain (PRD), located centrally in tau in a region containing an unusually high density of potential sites of proline-directed phosphorylation, with the two other modifications located in the first MTBD. Most of the modifications are known sites of phosphorylation in AD brain tau (Hanger et al., 2009) and/or are sites that have been shown to be phosphorylated in murine tau in wild-type and human APP transgenic mice (Morris et al., 2015). Although the average phosphate content of hyperphosphorylated insoluble tau in AD brains shows interindividual variation of between 3 and 15 mol phosphate per mol of tau (Kopke et al., 1993; Ksiezak-Reding et al., 1992), the range at the single molecule level, likely within a highly heterogeneous pool of tau species, is probably even greater. If the overall amount of tau phosphorylation correlates with pathogenicity, then the phosphomimetic tau mutant, with 18 pseudophosporylated sites, might be expected to broadly replicate the effects of some of the most extensively hyperphosphorylated AD-associated tau species. The mutants may also provide additional insight into the role of phosphorylation of residues within the specific domains targeted in this study, both of which are key regulatory regions involved in protein interactions (Ittner and Gotz, 2011; Kolarova et al., 2012; Mietelska-Porowska et al., 2014). Crucially, our phosphomimetic mutant also has a greater pseudophosphorylation load than PHP tau (10 substitutions), and the complement of modifications is largely nonoverlapping (Hundelt et al., 2011).

We find that some key properties of tau are altered in a largely phosphorylation-dependent manner in these mice, including reduced interactions with microtubules and membranes. These are consistent with established in vitro effects of phosphorylation at a variety of sites in tau, including some of those mutated here, although this particular combination of sites has not previously been studied in any context. We also see significant mislocalization of both tau mutants, with strong reductions in axonal tau and increases in somatodendritic tau in some neuron types in both lines. Structural changes in the PRD, rather than pseudophosphorylation, may thus be key, although there is also some evidence for earlier and more pronounced changes in the phosphomimetic tau knockin. Notably, despite these observed changes in tau properties, we could not detect pathological aggregation of tau in either line. We discuss the implications of these results with respect to the role of extensive tau phosphorylation on normal tau function and in neurodegenerative diseases.

2. Materials and methods

2.1. Generation of knockin mice expressing phosphomimetic and phosphodefective tau

Serine and threonine codons in human *MAPT* exon 9 (within a plasmid containing the whole *MAPT* coding region) were mutated to glutamate or alanine by QuikChangeII site-directed mutagenesis (Stratagene, La Jolla, CA, USA). Polymerase chain reaction (PCR) cloning was used to generate the targeting vectors (Fig. 1A) for each knockin (identical bar the mutations) using pEasy-Flox as a backbone (a gift from Profs. W. Müller and K. Rajewsky). Briefly, the 5′ arm (5′ to the Neo^r cassette) was generated by ligation of the mutant human *MAPT* exon 9 (either with 9E18 or 9A18 mutation sets) to sequences flanking the mouse *MAPT* exon 9, using restriction sites and flanking sequences introduced into the PCR primers so that flanking intronic regions remained unaltered. The 3′ arm was cloned as a single fragment. The flanking mouse genomic regions were amplified by PCR from C57BL/6J mouse bacterial artificial chromosomes (Children's Hospital, Oakland Research Institute). Linearized targeting vector was electroporated into C57BL/6-Thy1.1-derived Bruce 4 embryonic stem (ES) cells by the Babraham Institute Gene Targeting Facility. Correctly targeted G418-resistant clones for each knockin were identified by Southern blot analysis of *Spe*I-digested genomic DNA using flanking 5′ and 3′ probes (positions shown in Fig. 1A) and were injected into C57BL/6J-Tyrc-2J (albino) blastocysts and transferred to pseudopregnant women (C57BL/6JOlaHsd × CBA/Ca). Resulting chimeric male offspring were mated to C57BL/6J-Tyrc-2J women and germ line transmission of the mutant allele assessed by Southern blotting. Cre recombinase-mediated excision of the floxed neomycin-resistance cassette (Neo^r) was performed by mating to C57BL/6J deleter mice bearing a ubiquitously expressed X-linked Cre transgene (kindly provided by Miguel Constancia). Mice were PCR genotyped for presence of the knockin alleles using primers 5′-TTGGGGTCACCCTACTGACTTC-3′ and 5′-GACTGAGGAATGGTTCACAGCC-3′ (primer locations and representative results are shown in Fig. 1A and B). Normal Mendelian ratios were obtained from heterozygote crosses. Mice were bred to homozygosity so that mice expressing only each tau mutant were studied. All mice were bred, housed, and used in accordance with the UK Home Office Animals (Scientific Procedures) Act, 1986, under Project Licenses PPL 80/1778, 80/2254, and 70/7620.

2.2. Cell culture and transfection

Superior cervical ganglia (SCGs) obtained from P1 or P2 mouse pups were plated whole onto 3.5-cm tissue culture dishes precoated with poly-L-lysine (20 μg/mL for 1–2 hours; Sigma) and laminin (20 μg/mL for 1–2 hours; Sigma) for SCG explant cultures. For dissociated SCG cultures, ganglia were incubated in 0.025%

trypsin (Sigma) in PBS (without $CaCl_2$ and $MgCl_2$) for 30 minutes followed by 0.2% collagenase type II (Gibco) in PBS for 30 minutes before gentle trituration using a 1-mL plastic pipette tip. After a 2-hour preplating step (to remove non-neuronal cells), neurons were plated on poly-L-lysine and laminin-coated ibidi μ-dishes (Thistle Scientific). Explant and dissociated SCG cultures were maintained in Dulbecco's Modified Eagle's Medium with 4500 mg/L glucose and 110 mg/L sodium pyruvate (Sigma), supplemented with 10% fetal bovine serum (Sigma), 100 ng/mL 7S NGF, 1% penicillin and/or streptomycin, and 2-mM L-glutamine (all Invitrogen). Proliferation and viability of small numbers of non-neuronal cells were inhibited by 4-μM aphidicolin (Calbiochem). Separate ganglia and neurite fractions for immunoblotting were generated from explant cultures essentially as described previously (Gilley and Coleman, 2010). Briefly, ganglia were separated from their neurites with a scalpel. Neurites and ganglia were then collected separately, washed in PBS, lysed in 2× Laemmli buffer, and heated at 100 °C (10 minutes) before analysis.

For dissociated cortical neuron cultures, cortical tissue (with meninges removed) was dissected from P1 or P2 mouse pups and incubated in 0.025% trypsin for 20 minutes followed by gentle trituration using a 1-mL plastic pipette tip. The course cell suspension was then passed through a 70-μm strainer (Corning). Neurons were plated on 3.5-cm tissue culture dishes precoated with poly-L-lysine and laminin (as for SCGs) and maintained in Neurobasal Medium (Invitrogen) supplemented with 2% B27 supplement (Invitrogen), 1% penicillin and/or streptomycin, and 2-mM L-glutamine.

Chinese hamster ovary (CHO) cells were cultured in Ham's F12 medium (Invitrogen) supplemented with 10% fetal bovine serum, 1% penicillin and/or streptomycin, and 2-mM L-glutamine. CHO cells were transfected using Lipofectamine (Invitrogen) following the supplied instructions.

2.3. Reverse transcriptase PCR (RT-PCR)

RNA extraction and RT-PCR were performed essentially as described previously (Gilley et al., 2012). A region spanning murine *MAPT* exons 7 to 11 were amplified using primers 5′-CGTCCAACGCCACCAGGATCC-3′ and 5′-CTGGCTTGTGATGGATGTTCC-3′ for sequencing to confirm that only mutant mRNA is expressed in the homozygous knockin mice. A region spanning murine *MAPT* exons 10 to 13 were amplified using primers 5′-GAAGCTGGATCTTAGCAACGTCC-3′ and 5′-TTATTGACTGCCCTGGGAGCC-3′ for semiquantitative end point RT-PCR analysis of *MAPT* levels in the mutant mice. This was performed as described previously (Gilley et al., 2013). β-actin (*Actb*) transcripts, acting as the sample reference, were amplified using primers 5′- TGTTACCAACTGGGACGACA-3′ and 5′-ATGAGGTAGTCTGTCAGGTC-3′. *MAPT* exon numbering is based on accepted human *MAPT* gene structure (Andreadis et al., 1992).

2.4. Fractionation and dephosphorylation of brain lysates for immunoblot analysis

For crude extracts, whole brains from adult mice were mechanically homogenized using an Ultra-Turrax homogenizer in 1× TG lysis buffer consisting of 20-mM Tris (pH 7.5), 137-mM NaCl, 1-mM EGTA, 1% (v/v) Triton X-100, 10% (v/v) glycerol, 1.5-mM $MgCl_2$, 1-mM Na_3VO_4, 50-mM NaF, and cOmplete Mini protease inhibitor cocktail (Roche). Samples were centrifuged at 10,000 g for 5 minutes at 4 °C to pellet cell debris. The supernatant was diluted in 2× Laemmli sample buffer for immunoblot analysis.

Fractionation of brain lysates was performed essentially as described previously (Gilley et al., 2012) but with minor modifications. Dissected mouse cortices (one hemisphere) snap-frozen in liquid nitrogen were later homogenized on ice in 600-μL MES buffer (100-mM 2-(N-morpholino)ethanesulfonic acid (MES) pH 6.5, 0.5-mM $MgCl_2$, 1-mM EGTA, 1-M NaCl, 25-mM β-glycerophosphate, 50-mM imidazole, 20-mM NaF, 10-mM $Na_4P_2O_7$, and protease inhibitor cocktail (Sigma)) using an Ultra-Turrax homogenizer (20 seconds). Cellular debris was removed by centrifugation at 27,000 $g_{(av)}$ for 30 minutes at 4 °C and 350 μL of supernatant was then centrifuged at 100,000 $g_{(av)}$ for 1 hour at 4 °C. The entire pellet, containing insoluble tau, was then resuspended directly in 400 μL 2× Laemmli SDS-PAGE sample buffer and an aliquot of the 100,000 g supernatant, containing soluble tau, was diluted 10× into 2× Laemmli buffer. Fractions were assessed by immunoblotting.

For dephosphorylation assays, soluble fractions generated as mentioned previously (before the addition of Laemmli buffer) were dialyzed to 50-mM Tris pH 7.5 for 1 hour and then incubated with or without λ protein phosphatase (NEB Biolabs) for 2 hours at 30 °C. Reactions were stopped by boiling for 5 minutes. Equal amounts of phosphatase-treated and untreated lysates diluted in 2× Laemmli buffer were heated at 100 °C (10 minutes) and assessed by immunoblotting.

2.5. Endogenous microtubule-binding assay

We used a modification of an in situ microtubule-binding assay (Ding et al., 2006), essentially as described previously (Gilley et al., 2012; Rodriguez-Martin et al., 2013). Freshly dissected half brains (no cerebellum), or PBS-rinsed CHO cells transfected for 24 hours with plasmids (pEGFP-C1 backbone) expressing eGFP-tagged wild-type human tau (eGFP-htau), human 9E18tau (eGFP-h9E18tau), or human 9A18tau (eGFP-h9A18tau), were homogenized in warm microtubule stabilizing buffer (80-mM PIPES/KOH, pH 6.8, 1-mM GTP, 1-mM $MgCl_2$, 1-mM EGTA, 0.5% Triton X-100, 30% glycerol, 0.5-μM okadaic acid and 10-μM Taxol and 1× protease inhibitor cocktail). Homogenized samples were centrifuged at 5000 $g_{(av)}$ for 10 minutes at room temperature (RT). An aliquot of the supernatant was retained as the postnuclear lysate "input" fraction. The remaining postnuclear lysate was then centrifuged at 100,000 $g_{(av)}$ for 1 hour at 25 °C with the resulting supernatant representing the "soluble" fraction and the pellet the "microtubule" fraction The pellet was rinsed twice in PBS before being resuspended in the same volume of microtubule-stabilizing buffer as the amount of supernatant recovered. Fractions were diluted in 2 volumes of 2× Laemmli buffer, heated at 100 °C for 10 minutes, and equal volumes assessed by immunoblotting. Prewarming microtubule-stabilizing buffer to 37 °C (rather than RT) before addition to the half brains in this study may account for the slightly higher microtubule fraction yields obtained compared to those seen previously (Gilley et al., 2012).

2.6. Cell fractionation for membrane association assays

Mouse cortical tissue was disrupted in hypotonic buffer (10-mM sodium bicarbonate containing 20-mg/mL deoxyribonuclease I (DNase I), 1-mM sodium orthovanadate, and Complete protease inhibitor cocktail) by sonication using 5 strokes with probe sonicator on ice. Samples were then processed as described previously (Pooler et al., 2012). Briefly, lysates were centrifuged at 720 g for 5 minutes at 4 °C. The supernatant was then removed and centrifuged at 100,000 g for 1 hour at 4 °C. The final supernatant (cytosolic fraction) and the pellet (membrane fraction) were resuspended in Laemmli sample buffer and heated at 100 °C (10 minutes) before immunoblot analysis.

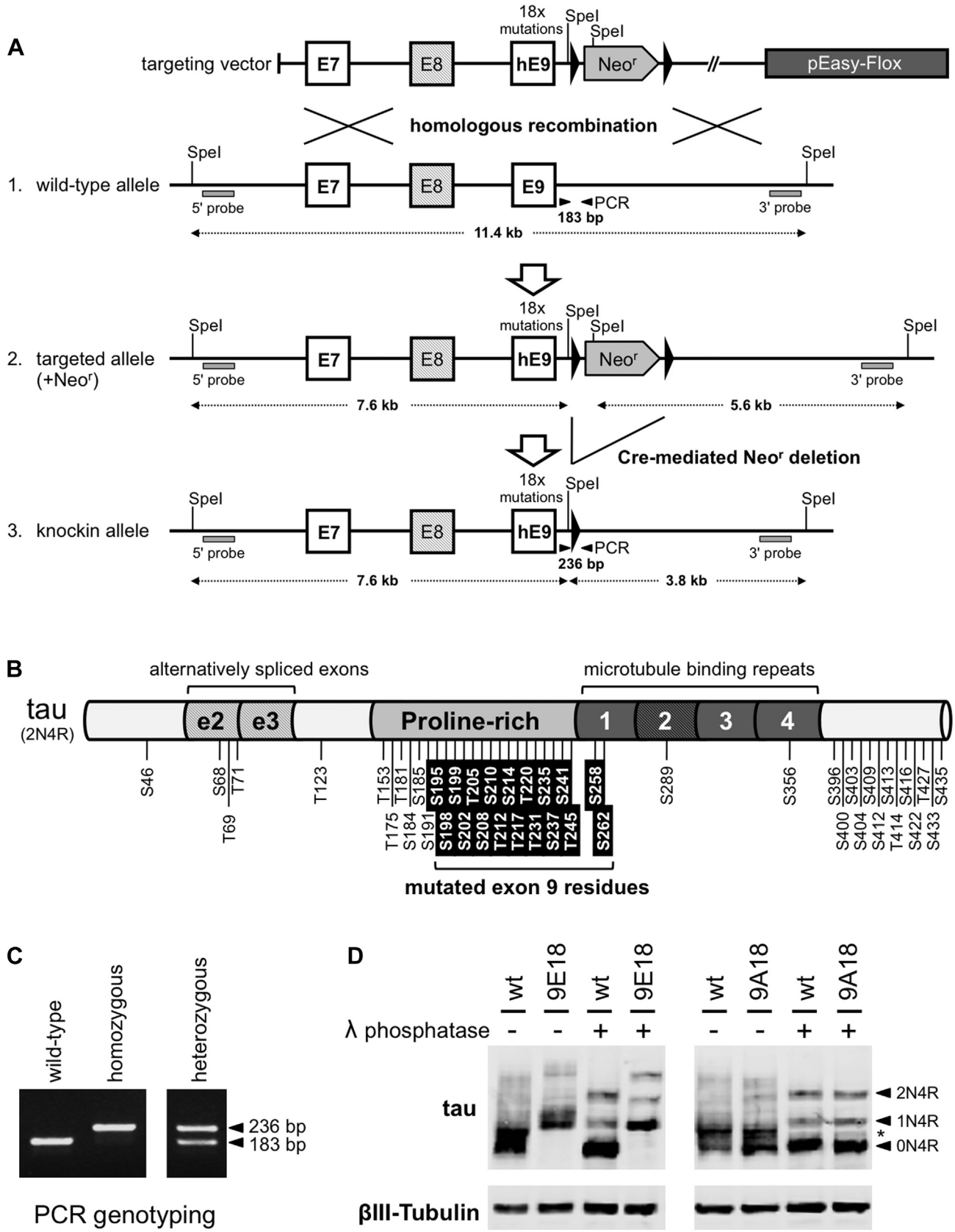

Fig. 1. Generation of *Mapt*-9E18 and *Mapt*-9A18 phosphomimetic and phosphodefective tau knockin mice. (A) Targeting strategy used to replace murine *Mapt* exon 9 (E9) with human *MAPT* exon 9 (hE9) bearing 18 phosphomimetic or phosphodefective mutations to generate murine *Mapt*-9E18 or *Mapt*-9A18 knockin alleles. The targeting vector and corresponding region of the murine *Mapt* locus are shown at key stages of the process (not to scale). The neomycin resistance cassette (Neo^r) was removed by in vivo Cre-mediated recombination via flanking loxP sites (large arrowheads). ES cell clones and founder mice were screened by Southern blotting of *Spe*I-digested genomic DNA using 5′ and 3′ probes

2.7. Immunoblotting

Boiled samples were resolved in 10% or 12% (w/v) polyacrylamide gels before transfer onto Immobilon-FL PVDF membrane (Millipore). Membranes were blocked with 5% (w/v) nonfat dried milk (1 hour, RT) and then probed with the following primary antibodies overnight at 4 °C: DAKO antitau (1:5000–10,000); TP007 anti-tau (1:1000) (Davis et al., 1995); AT270 (Innogenetics, 1:1000) recognizing phospho-T181 tau; PHF-1 recognizing phospho-S396/S404 tau (gift from P. Davies, 1:2000); antibodies recognizing tau phosphorylated at S356, S396, S404, S409, and S422 tau (Invitrogen, 1:1000–2000); antisynaptophysin (DAKO or Abcam Ab8049, 1:1000); TUJ1 monoclonal antineuronal class III β-tubulin (Covance, 1:10,000–15,000); and AC15 anti-β-actin (Abcam, 1:5000) (for all tau antibodies numbering is as in human 2N4R tau). Blots were washed and probed with AlexaFluor 680-conjugated antimouse (Molecular Probes, Eugene, OR, USA) or IRDye800-conjugated antirabbit (LI-COR Biosciences, Lincoln, NC, USA) donkey secondary antibodies (both 1:5000) for 1–2 hours at RT. Immunoblots were visualized and quantified using the Odyssey imaging system (LI-COR Biosciences). The use of different percentage gels and/or varying run lengths likely accounts for the differential resolution of tau species (particularly for 9E18tau) which is apparent between different experiments. Quantities of extract required to ensure immunodetection in the dynamic linear range were determined empirically. Standard curves for antibodies used in key quantitative analyses are shown in Supplementary Fig. 7.

2.8. Gallyas silver-stain and immunohistochemical and/or immunofluorescent staining

Mouse brains and spinal cords were fixed in 10% formalin for at least 24 hours before dehydration and embedding in paraffin. Gallyas silver staining of tissue sections (7-μm thick) for identification of NFTs was performed as described previously (Leroy et al., 2007).

Immunohistochemical labeling of tissue sections was performed using the ABC method. Sections were treated with 0.3% H_2O_2 to inhibit endogenous peroxidase, blocked in 10% (v/v) normal horse serum in TBS (0.01-M Tris, 0.15-M NaCl, pH 7.4), and incubated overnight with diluted mouse monoclonal phosphorylation-independent antimurine tau mTau2 (a generous gift from M. Mercken, Johnson & Johnson, Beerse, Belgium) or B19 antibodies (Brion et al., 1991), or AT270 or PHF-1 phosphorylation-dependent antibodies (described previously). Sections were then incubated with biotin-conjugated goat antirabbit or horse antimouse antibodies followed by ABC complex (Vector Laboratories). Peroxidase activity was developed using diaminobenzidine as the chromogen. The optical density of tau staining in different layers of the cerebellum was calculated from images (40× objective) using the public domain ImageJ software (rsb.info.NIH.gov/nih-image/).

For immunofluorescent labeling of tissue sections, rehydrated sections were blocked in 10% (v/v) normal horse serum in TBS and incubated overnight with monoclonal mTau2 and rabbit polyclonal anti-neurofilament-light (NF-L) antibody (NA1214, Enzo life science, Belgium). Sections were then incubated with biotin-conjugated horse antimouse and Alexa594-conjugated antimouse secondary antibodies followed by ABC complex. Biotin-labeled signal was amplified by Tyramid signal amplification Fluorescein system (Perkin Elmer). Sections were counterstained by DAPI (4',6-diamidino-2-phenylindole) before mounting in gelvatol.

For immunofluorescent staining of dissociated SCG and cortical neurons, cells were fixed in 4% paraformaldehyde for 20 minutes, permeabilized in 1% Triton X-100 in PBS for 10 minutes, and blocked in 50% goat serum in PBS containing 1% BSA for 30 minutes, before being coincubated with DAKO antitau and TUJ1 antineuronal class III β-tubulin antibodies (both 1:1000 in PBS, 1% BSA for 1 hour) followed by Alexa488-conjugated antirabbit and Alexa568-conjugated antimouse secondary antibodies (1:200 in PBS, 1% BSA for 1 hour). Cells were mounted in Vectashield containing DAPI (Vector Laboratories) for counterstaining of nuclei.

For immunofluorescent staining of transfected CHO cells, cells were fixed in 4% paraformaldehyde 24 hours after transfection, blocked in 1% Triton X-100, 10% fetal bovine serum in PBS for 20 minutes, and then incubated with mouse monoclonal DM1A anti-α-tubulin (Invitrogen) for 1 hour followed by an antimouse Texas Red-coupled secondary antibody for 1 hour.

Images of stained sections were acquired using a Zeiss Axioplan microscope and an Axiocam HRc camera. Bright field and fluorescence images of SCG or cortical cultures were captured on an Olympus IX81 inverted fluorescence microscope using a Soft Imaging Systems F-View camera linked to a PC running Soft Imaging System software. Fluorescence microscopy of transfected COS cells was performed using an Axioskop microscope (Zeiss), equipped with a CoolSnap HQ camera (Photometrics). Images were processed using Adobe Photoshop Elements 4.0 for presentation.

2.9. Measurements of cross-sectional areas of hippocampal regions

The public domain ImageJ software (rsb.info.NIH.gov/nih-image/) was used to calculate the cross-sectional area of different regions of the hippocampus after manual delineation of their borders on low magnification images (5× objective) of diaminobenzidine-stained sections at Bregma lateral 1.1–1.3 mm probed with the B19 total tau antibody.

2.10. Analysis of mitochondrial transport

Mitochondrial transport in ex vivo tibial nerve axons of 5- to 9-month-old wild-type, *Mapt-9E18*, or *Mapt-9A18* mice heterozygous for the *Thy1-mitoCFP-S* (Mito-S) transgene (Misgeld et al., 2007) was assessed essentially as described previously (Andrews et al., 2010; Gilley et al., 2012).

2.11. Statistical analysis

Appropriate statistical tests, as described in the text or figure legends, were performed using Prism software (GraphPad Software

bordering the targeted region (restriction fragment sizes are shown). PCR primers (small arrowheads) flanking the single retained loxP site after Neo^r deletion were used for subsequent PCR genotyping of mice (see the following). (B) Illustration showing the 18 serine and threonine residues (white text on black background) that we mutated to glutamate or alanine. All are potential phosphorylation sites that are conserved between human and mouse. Other common phosphorylation sites and key domains in human tau are also labeled. Numbering relates to human 2N4R tau (441 amino acids). The equivalent residues in murine tau are S184, S187, S188, S191, T194, S197, S199, T201, S203, T206, T209, T220, S224, S226, S230, T234, S247, and S251. (C) Typical PCR genotyping results for wild-type and homozygous knockin mice (left) compared to a heterozygous mouse (right—not assessed in this study). (D) Representative immunoblots (of n = 3) of total tau and βIII-tubulin, acting as a sample reference, in soluble fractions of brain lysates from wild-type (wt), *Mapt*-9E18 or *Mapt*-9A18 mice (aged 8 months), before or after treatment with λ phosphatase. Positions of the predominant adult murine tau isoforms (0N4R, 1N4R, and 2N4R—arrowheads) and a known N-terminally-cleaved species [(Takuma et al., 2003)—asterisk] are indicated. Abbreviation: ES, embryonic stem; PCR, polymerase chain reaction.

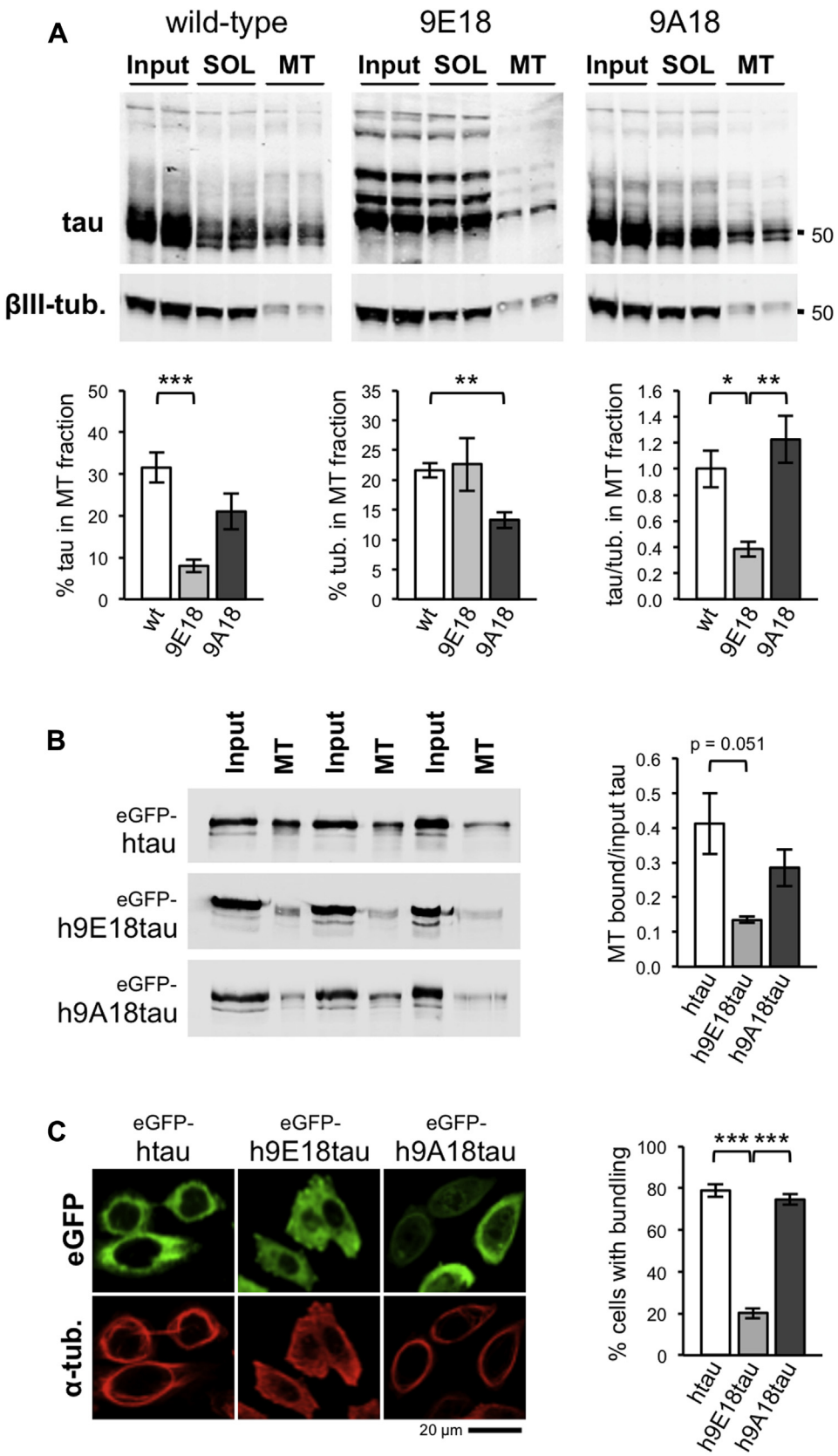

Fig. 2. Effects of 9E18 and 9A18tau mutations on tau-microtubule relationships. (A) Representative immunoblots showing total tau (DAKO antibody) and βIII-tubulin (βIII-tub.) levels in whole postnuclear brain extracts (Input) and derived soluble (SOL) and microtubule (MT) fractions from wild-type, *Mapt*-9E18, and *Mapt*-9A18 mice (aged 11–12 months). Graphs show the proportion of tau and βIII-tubulin in the microtubule fraction (as a percentage of soluble and microtubule fractions combined) and the ratio of tau to βIII-tubulin (tau/tub.) in the microtubule fraction based on data from n = 12 wild-types (wts) (pooled from each knockin line which were not significantly different) and n = 7 for each knockin. Means ± SEM are plotted with conversion of the tau/βIII-tubulin ratio data relative to a wild-type mean set at 1. $^{*}p < 0.05$, $^{**}p < 0.01$, $^{***}p < 0.001$, Kruskal-Wallis tests with Dunn's

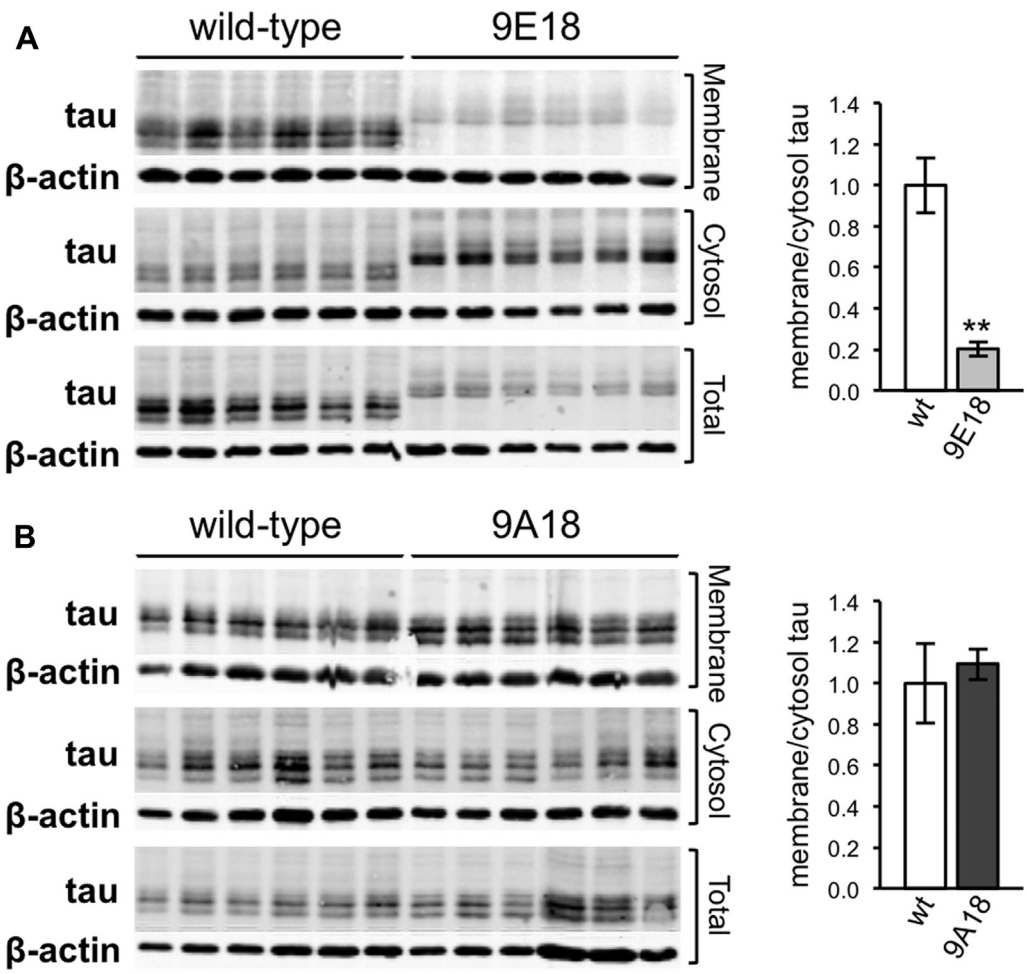

Fig. 3. Reduced membrane association of 9E18tau, but not 9A18tau in brains. Immunoblots showing total tau and β-actin levels in total lysates and cytosolic and membrane fractions derived the cortices of matched pairs (n = 6) of (A) wild-type and *Mapt*-9E18 knockin mice, and (B) wild-type and *Mapt*-9A18 knockin mice aged 3.5–9 months. Graphs show the ratio of tau in the membrane fraction compared to that in the cytosol fraction for the knockins as a proportion of that of their matched wild-type controls. Means ± SEM are plotted after conversion of the data sets relative to a wild-type mean set at 1. $^{**}p < 0.01$, Mann-Whitney test. Abbreviation: SEM, standard error of the mean.

Inc, La Jolla, CA, USA). A p value of >0.05 was considered not significant (ns) and $^{*}p < 0.05$, $^{**}p < 0.01$, and $^{***}p < 0.001$.

3. Results

3.1. Generation of knockin mice expressing phosphomimetic and phosphodefective tau

We generated complementary phosphomimetic and phosphodefective tau knockin mice using a homologous recombination strategy targeting the endogenous murine *MAPT* gene. In short, exon 9 of the mouse *MAPT* gene, encoding the PRD and first MTBD, was replaced with a mutated human *MAPT* exon 9 (84/88 amino acid identity with mouse exon 9) in which 18 conserved serine and threonine codons were changed to specify glutamate to mimic phosphorylation, or alanine to prevent phosphorylation (Fig. 1A and B). The two sets of tau mutations are hereafter referred to as 9E18 and 9A18, respectively. By incorporating the mutations directly into the endogenous *MAPT* gene, we anticipated that in mice homozygous for the modified alleles, the modified proteins would be expressed at close to physiological levels, only in appropriate cell types, with a normal pattern of alternative splicing, and in the absence of any wild-type murine tau. This should exclude the potentially confounding influences of tau overexpression and/or changes to tau isoform ratios that are often a feature of cDNA knockin and transgene strategies (Gilley et al., 2011). Crucially, this further differentiates these mice from PHP tau transgenic mice (Hundelt et al., 2011).

Southern blotting confirmed correct targeting of the *Mapt*-9E18 and *Mapt*-9A18 knockin alleles, and mice were PCR genotyped after Cre-mediated deletion of the neomycin resistance cassette in vivo (Fig. 1A and C). Only mice homozygous for either the *Mapt*-9E18 or

multiple comparisons post hoc analysis. Mice were 12 months old ± 1 month. (B) Representative immunoblots showing levels of exogenous eGFP-htau, eGFP-h9E18tau, or eGFP-h9A18tau (GFP antibody) in whole postnuclear extracts (Input) and derived MT fractions from transfected CHO cells. The graph shows the proportion of tau in the microtubule fractions relative to input. Means ± SEM are plotted (n = 3). Statistical significance was tested using Kruskal-Wallis test with Dunn's multiple comparisons post hoc analysis. (C) Representative confocal images of CHO cells 24 hours after transfection with eGFP-htau, eGFP-h9E18tau, or eGFP-h9A18tau constructs showing eGFP fluorescence and the distribution of α-tubulin (α-tub.). Microtubule bundling is seen as thick circular rings of α-tubulin. The graph shows the percentage of transfected CHO cells displaying clear bundling. Means ± SEM are plotted (n ≥ 9 independent transfections). $^{***}p < 0.001$, one-way analysis of variance with Tukey's multiple comparisons post hoc analysis. Abbreviation: SEM, standard error of the mean.

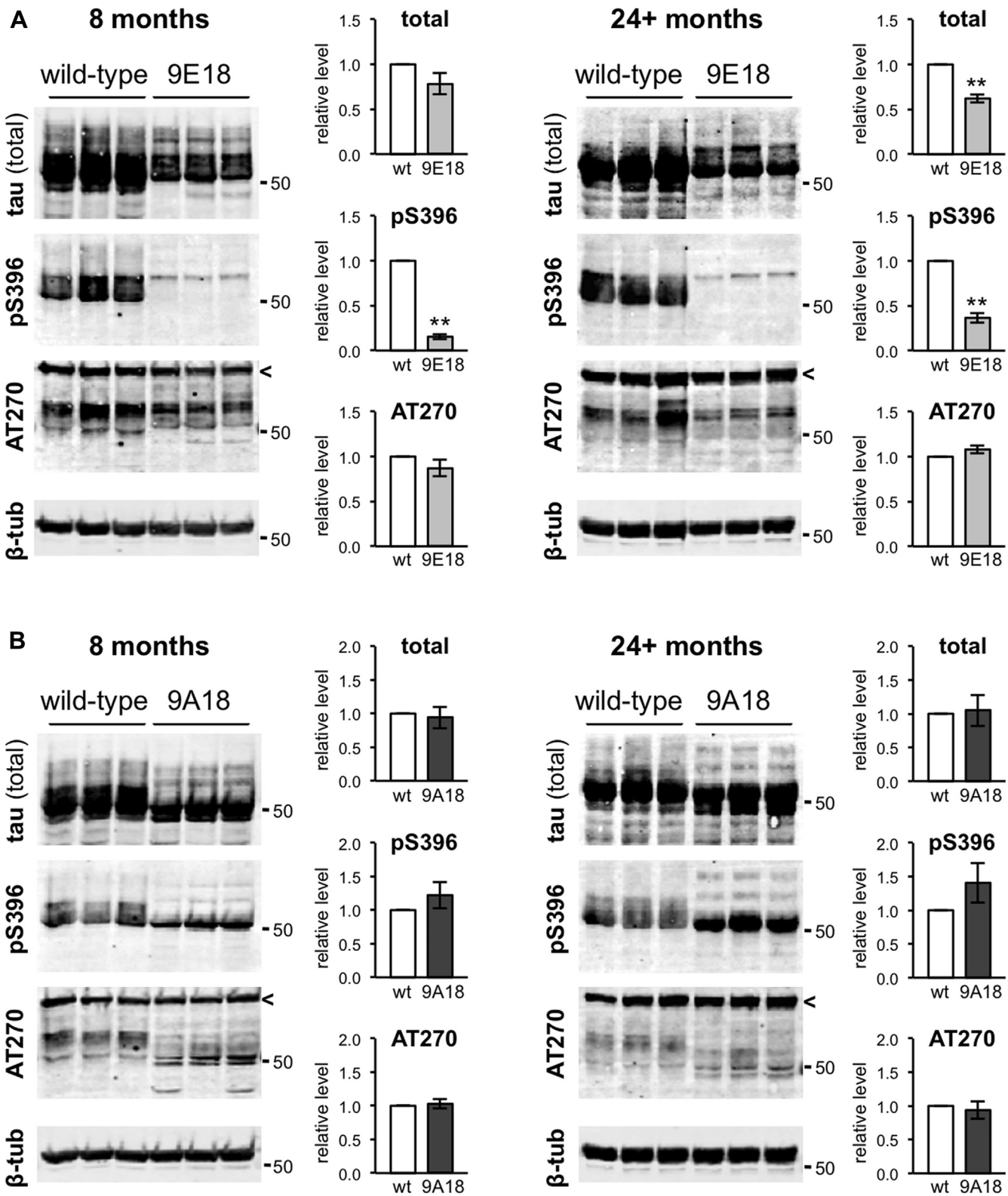

Fig. 4. Phosphorylation status of 9E18tau and 9A18tau in soluble fractions of brain extracts from *Mapt*-9E18 and *Mapt*-9A18 mice aged 8 or 24 months. Representative immunoblots and quantification of relative levels of total tau (DAKO antibody) and tau phosphorylated at murine residues equivalent to human S396 (pS396 antibody) and T181 (AT270 antibody) in soluble fractions of brain extracts from matched wild-type (wt) and *Mapt*-9E18 mice (A), and wild-type (wt) and *Mapt*-9A18 mice (B) aged 8 months or 24–26 (24+) months. βIII-tubulin (β-tub) acted as a loading reference. Graphs show levels of total tau (normalized to βIII-tubulin) and the relative level of phosphorylation at different phosphoepitopes (normalized to total tau) in knockin brains as a ratio of that in wild-type brains. The ratio of each knockin sample relative to its paired wild-type control (individually set at 1) was calculated to eliminate session-to-session technical variability. Means ± SEM are plotted. Data were quantified from n = 4 matched pairs at 8 months and n = 5 matched pairs at 24–26 months. $^{**}p < 0.01$, paired *t* tests (ratios of paired values). Migration of a 50-kDa size marker is shown to the right of the blots. Only the low molecular weight (LMW) tau species (45–65 kDa) were included in this analysis. High molecular weight (HMW) tau bands (>90 kDa) were detected, but they represent only a minor proportion of the total tau and intergenotype differences matched those seen for LMW tau. An HMW nonspecific band (<) is evident on the AT270 blots. Abbreviation: SEM, standard error of the mean.

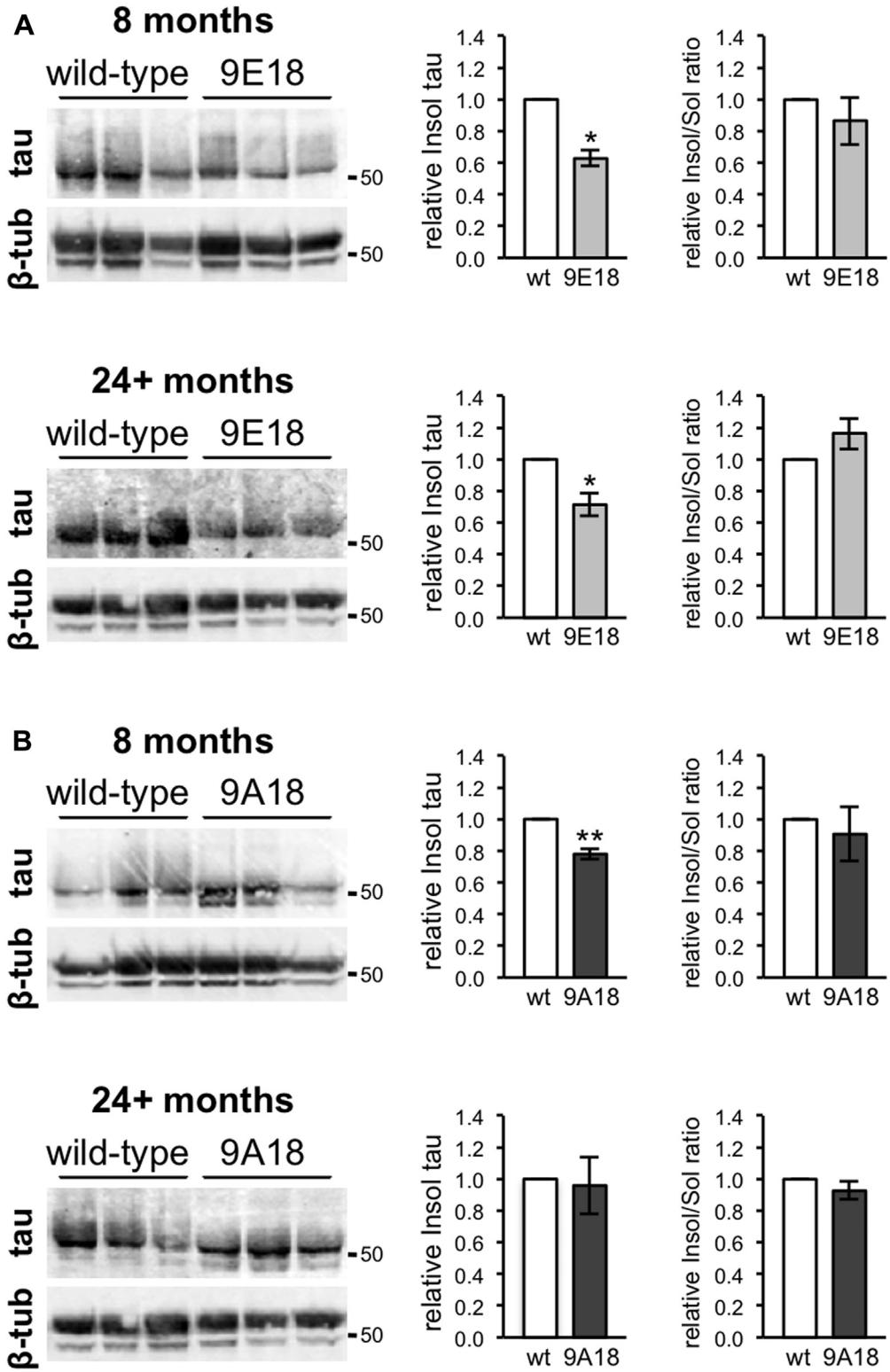

Fig. 5. No accumulation of insoluble 9E18tau or 9A18tau in brains of knockin mice at 8 or 24 months. Representative immunoblots and quantification of relative levels of total tau in insoluble fractions of brain extracts from matched wild-type and *Mapt*-9E18 mice (A), and wild-type and *Mapt*-9A18 mice (B) aged 8 months or 24–26 months. βIII-tubulin (β-tub) acted as a loading reference. Graphs show levels of total tau (normalized to βIII-tubulin) and the ratio of insoluble to soluble tau (Insol/Sol) in knockin brains as a ratio of that in wild-type brains. The Insol/Sol tau ratio was calculated by matching insoluble fractions to their soluble counterparts (Fig. 4). Insoluble tau actually represents less than 5% of total brain tau (not shown). The ratio of each knockin sample relative to its paired wild-type control (individually set at 1) was calculated to eliminate session-to-session technical variability. Means ± SEM are plotted. Data were quantified from n = 4 matched pairs at 8 months and n = 5 matched pairs at 24–26 months for each line. Means ± SEM are plotted. $^{*}p < 0.05$, $^{**}p < 0.01$, paired *t* tests (ratios of paired values). The position of a 50-kDa size marker is shown to the right. Only LMW tau species (45–65 kDa) were detected. Abbreviations: LMW, low molecular weight; SEM, standard error of the mean.

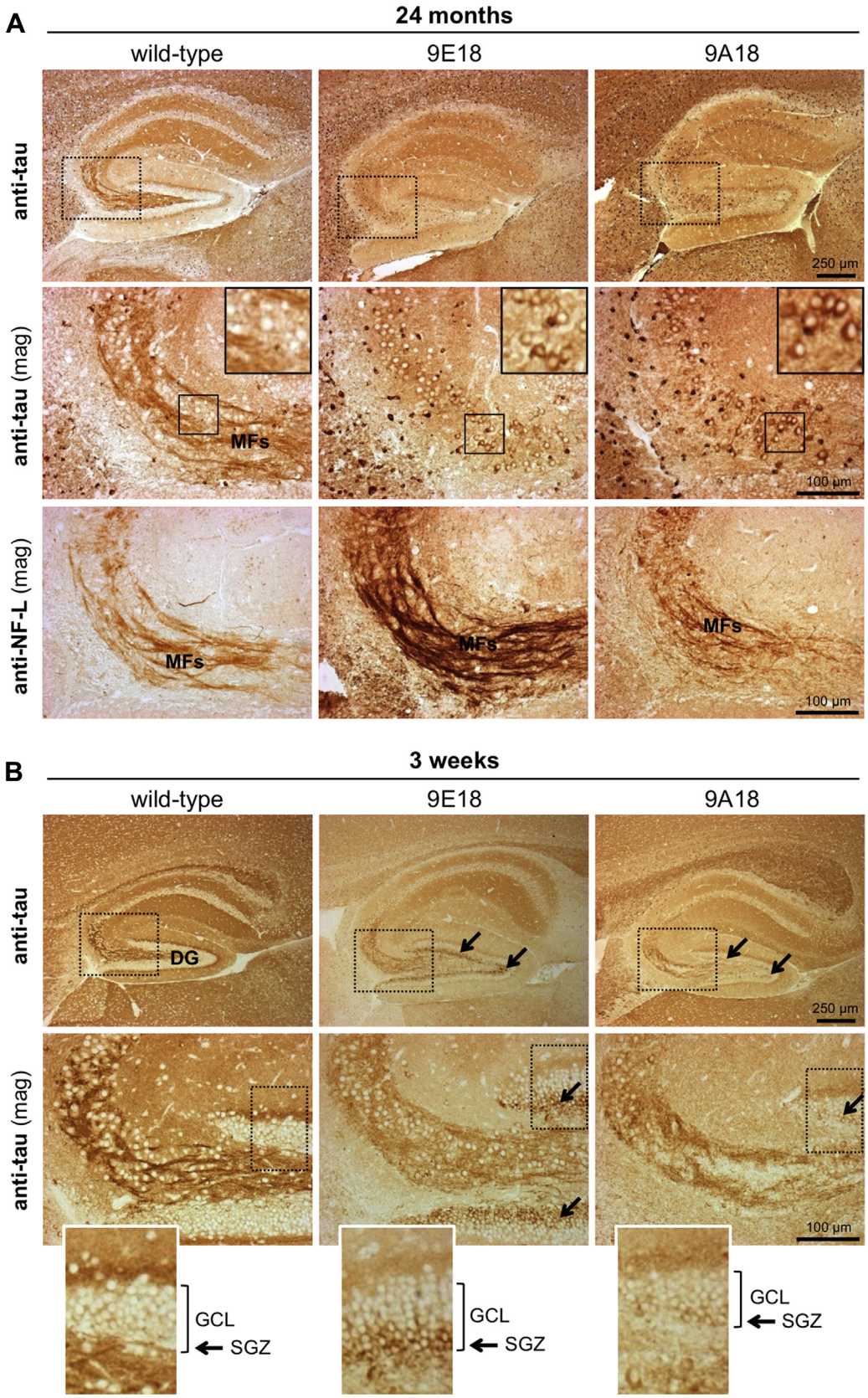

Fig. 6. Age-related changes in subcellular distribution of 9E18tau and 9A18tau in the hippocampus of knockin mice. Immunohistochemical staining for total tau and neurofilament-L (NF-L) on brain tissue sections encompassing the hippocampus of wild-type, *Mapt*-9E18, and *Mapt*-9A18 mice at 24 months (A) and at 3 weeks (B) reveals qualitative changes in the relative distribution of the mutant tau proteins (N.B. this is separate from global differences in absolute staining intensity which likely reflect session-to-session variation in the

Mapt-9A18 knockin alleles, hereafter referred to as *Mapt*-9E18 and *Mapt*-9A18 mice, were examined in this study. Sequencing of *Mapt* RT-PCR products confirmed that only the relevant mutant *Mapt* mRNA is detectable in the brains of the *Mapt*-9E18 and *Mapt*-9A18 mice, meaning that only phosphomimetic 9E18tau or phosphodefective 9A18tau is expressed.

Adult mice express primarily 4R tau isoforms and immunoblotting of phosphatase-treated brain lysates revealed that the ratio of the 0N4R, 1N4R, and 2N4R tau isoforms in *Mapt*-9E18 and *Mapt*-9A18 mice is broadly similar to that in wild-type mice (Fig. 1D). Thus, splicing is largely unaffected by either set of mutations. However, retarded electrophoretic mobility appears to be an inherent property of 9E18tau, rather than the result of increased phosphorylation at nonmutated sites, as it remains evident in phosphatase-treated samples (Fig. 1D). Unexpectedly, steady-state levels of 9E18tau in the brain are significantly lower than those of nonmutant tau in wild-type brains (49.5 ± 7.7% of wild-type levels after normalization to βIII-tubulin, $p = 0.043$ paired *t* tests [ratios of paired values], n = 3). In contrast, migration of 9A18tau is similar to nonmutant tau in wild-type mice (Fig. 1D), and its steady-state level is not significantly altered (105.6 ± 7.9% of wild-type levels, $p = 0.570$, n = 3). Similar relative expression patterns for the mutant proteins were consistently detected in different brain extract preparations and fractions, irrespective of the age of the animals, the method of preparation, or the total tau antibody used (see below). Intriguingly, RT-PCR analysis revealed an opposite trend for the mutant *Mapt* mRNAs (Supplementary Fig. 1); *Mapt*-9E18 mRNA levels in *Mapt*-9E18 brains are modestly higher than nonmutant *Mapt* mRNA levels in wild-type brains (118.9 ± 3.5% of control levels after normalization to *Actb* mRNA, $p = 0.011$ paired *t* tests [ratios of paired values], n = 4), whereas *Mapt*-9A18 mRNA levels in *Mapt*-9A18 brains are almost halved (53.5 ± 4.9%, $p = 0.006$, n = 4).

3.2. Differential effects of 9E18 and 9A18 mutations on tau-microtubule relationships

The ability of tau to bind to and stabilize microtubules is influenced by phosphorylation (Bramblett et al., 1992, 1993; Busciglio et al., 1995; Wagner et al., 1996) and by synthetic mutations that either mimic or prevent phosphorylation (Rodriguez-Martin et al., 2013). Therefore, we evaluated endogenous association of 9E18tau or 9A18tau with microtubules in the brains of *Mapt*-9E18 and *Mapt*-9A18 mice (Fig. 2A). The amount of 9E18tau in microtubule fractions from *Mapt*-9E18 brains is reduced relative to that of wild-type tau in control brains, consistent with extensive pseudo-phosphorylation of tau severely disrupting its ability to bind to microtubules. Intriguingly, however, the relative paucity of microtubule-associated phosphomimetic tau has no effect on the overall size of the microtubule fraction as levels of neuron-specific βIII-tubulin in the *Mapt*-9E18 samples are similar to those from controls. As a result, there is a large reduction in the ratio of tau to βIII-tubulin in the *Mapt*-9E18 microtubule fractions. Conversely, a statistically significant reduction in the size of the microtubule fractions from *Mapt*-9A18 mouse brains, based on βIII-tubulin yield, suggests that 9A18tau is defective for microtubule binding and/or microtubule stabilization in some way, although there is potentially a much more modest reduction in the amount of the mutant that is actually associated with microtubules (not statistically significant due to sizable variation within the set) and a largely unaltered ratio of tau to βIII-tubulin. These data suggest that both mutants are dysfunctional for microtubule binding and/or microtubule stabilization to some extent, but that the relationship is different for each and is complex.

Any potential reduction in the amount of 9A18tau in the microtubule fractions from *Mapt*-9A18 brains was somewhat unexpected, given we previously found a related, but distinct, human phosphodefective tau mutant, A18tau, to be increased in transfected CHO cell microtubule fractions (Rodriguez-Martin et al., 2013). We therefore compared recovery of microtubule-associated eGFP-tagged human wild-type tau (eGFP-htau), human 9E18tau (eGFP-h9E18tau), and human 9A18tau (eGFP-h9A18tau) from transfected CHO cells (Fig. 2B). Importantly, the relative amounts of eGFP-h9E18tau and eGFP-h9A18tau in the CHO microtubule fractions broadly matched those of 9E18tau and 9A18tau in mouse brains (compare Fig. 2A and B). Furthermore, consistent with the known correlation between reduced microtubule-binding capacity and a reduced ability of tau to induce microtubule bundling (Kanai et al., 1989; Rodriguez-Martin et al., 2013; Wagner et al., 1996), we found that eGFP-h9E18tau is unable to efficiently induce microtubule bundling in CHO cells, whereas similar overexpression of eGFP-h9A18tau promotes bundling that is comparable to wild-type tau (Fig. 2C).

3.3. Reduced membrane association of 9E18tau but not 9A18tau

A proportion of endogenous tau has previously been shown to associate with membranes in a variety of cell lines and in rat cortical neurons, and this can be inhibited by phosphorylation (Arrasate et al., 2000; Brandt et al., 1995; Maas et al., 2000; Pooler et al., 2012). We therefore compared tau levels in membrane and cytosol fractions of cortical extracts from adult wild-type, *Mapt*-9E18, and *Mapt*-9A18 mice by immunoblotting (Fig. 3). We found that the proportion of 9E18tau in membrane fractions is substantially reduced relative to nonmutant tau in wild-type mice, whereas the proportion of 9A18tau associating with membranes is essentially normal. These results confirm that a proportion of tau is membrane-associated in vivo and that this association is specifically disrupted by phosphomimetic mutations. This is entirely consistent with phosphorylation inhibiting the association of tau with membranes in mice.

3.4. Reduced phosphorylation of 9E18tau, but not 9A18tau, in mouse brain

We previously proposed a mechanistic link between reduced microtubule association of P301L-equivalent mutant murine tau in "P301L" tau knockin mice and its relative hypophosphorylation (Gilley et al., 2012). We therefore assessed whether similar intrinsic differences in phosphorylation of 9E18tau or 9A18tau occur in the brains of *Mapt*-9E18 and *Mapt*-9A18 mice, and/or whether there are

staining process and/or differences in steady-state tau levels in the different genotypes). Boxed regions bordered by black dashed lines in each part are magnified in image panels immediately below. (A) Staining for tau is essentially undetectable in NF-L-positive mossy fibers (MFs) in the CA3 and CA4 regions (middle panels) of 24-month-old *Mapt*-9E18 and *Mapt*-9A18 mice. Pyramidal neurons in the same region also appear to show more intense somatodendritic tau immunoreactivity in both knockins. Small boxed regions bordered by solid black lines in the middle row of panels are magnified top right of the same panel for clearer visualization of the soma of the pyramidal neurons. Small, intensely stained cells, seen in all mice, are tau-positive oligodendrocytes (Migheli et al., 1988). (B) Somal tau immunoreactivity is increased in cells in the subgranular zone (SGZ) and neighboring cells in the granule cell layer (GCL) of the DG in 3-week-old *Mapt*-9E18 mice and to a lesser extent in *Mapt*-9A18 mice (arrows and magnified panels, bottom row). Images are representative of at least n = 3 of each genotype at each age. There was no obvious deviation from the observations in the aged group over a range of ages spanning 21–28.5 months. Similar results were obtained using two independent total tau antibodies (mTau2, shown, and B19).

age-related changes in phosphorylation that could have additional functional implications.

Soluble fractions of whole brain extracts from *Mapt*-9E18 and *Mapt*-9A18 mice aged 8 or 24–26 months were probed with a variety of phosphorylation-dependent tau antibodies raised against human tau epitopes that are conserved in murine tau. The number of epitopes we could examine was limited as many available antibodies recognize sites that are already modified in the tau mutants. Nevertheless, outside of the targeted region, we found that 9E18tau was markedly hypophosphorylated at the murine equivalent of human S396 at both ages, even accounting for reduced steady-state levels of 9E18tau (Fig. 4A). In contrast, we saw no significant difference in 9A18tau phosphorylation at this site at either age (Fig. 4B). Similar results were obtained with the PHF-1 antibody, which recognizes murine tau phosphorylated at residues equivalent to human S396 and/or S404, but a general absence of reactivity to a human S404 phosphorylation-dependent antibody suggests phosphorylation is largely restricted to the S396-equivalent residue in these mice (not shown). Therefore, as with "P301L" mutant murine tau, reduced microtubule-binding capacity of 9E18tau correlates with hypophosphorylation at this site.

Immunoreactive bands were also detected with phosphorylation-dependent antibodies recognizing human tau T181 (AT270) and S422, but phosphorylation of each mutant was similar to wild-type tau at both ages (Fig. 4 and not shown). Finally, none of the samples showed significant reactivity to human S356 and S409 phosphorylation-dependent antibodies (not shown). This implies these two sites are not normally phosphorylated in mice. Although reduced phosphorylation has thus only been formally shown at the murine equivalent of human S396, the more defined banding pattern consistently seen for 9E18tau on blots probed with total tau antibodies could reflect hypophosphorylation at other, untested sites. Crucially, no significant age-related changes in phosphorylation were observed for either of the tau mutants (Fig. 4).

3.5. *Absence of tau aggregation in* Mapt-*9E18 and* Mapt-*9A18 mouse brain*

To investigate whether either knockin mouse line showed any aggregation of insoluble tau during aging, we assessed tau levels in insoluble fractions of whole brain extracts from wild-type and knockin mice aged 8 or 24 months (counterparts to the soluble fractions described in Section 3.3). These fractions were generated using a method that maximizes the yield of insoluble, highly phosphorylated tau (Hanger et al., 1998, 2007). We found that insoluble 9E18tau was reduced relative to wild-type tau at both ages (Fig. 5A), and insoluble 9A18tau was reduced at 8 months, but not at 24 months (Fig. 5B). However, we found no significant difference in the ratio of insoluble to soluble tau for either mutant at either age (Fig. 5), suggesting the reductions in absolute levels just reflect differences in steady-state levels of the mutants. Phosphorylation at residues equivalent to human tau T181, S356, S396, S404, S409, and S422 was also either undetectable or equivalent to that in soluble fractions (not shown), and no distinct hyperphosphorylated tau species with retarded electrophoretic mobility were visible. Together, these data suggest that, up to 24 months of age, neither mutant tau species forms pretangle aggregates in the brains of *Mapt*-9E18 or *Mapt*-9A18 mice.

3.6. *Altered subcellular distribution of 9E18tau and 9A18tau in the absence of any tangle pathology or other toxic effects*

Consistent with the absence of any increase in insoluble tau in the brains of aged knockin mice, we did not detect any tau aggregates and/or tangle pathology in either knockin line up to the age of 24 months using Gallyas staining or immunohistochemical staining with the phosphorylation-dependent PHF-1, AT270, or AT8 antibodies (not shown). In addition, whole-brain synaptophysin levels are unaltered in both knockins at 24 months suggesting the mutant proteins are not overtly toxic to synapses (Supplementary Fig. 2A and B). However, staining for total tau revealed intriguing age-related changes in the relative subcellular distribution of the mutant proteins in both lines.

Clear qualitative changes in tau distribution were seen in both the hippocampus and cerebellum. Changes in the hippocampus are most evident in 24-month-old mice where tau staining of the unmyelinated, small caliber granule cell axons of the mossy fiber tract in the stratum lucidum of the CA3 and/or CA4 regions is essentially absent in both mutants (NF-L staining confirming mossy fibers are present) and where immunoreactivity of pyramidal neuron cell bodies in the adjacent and/or underlying stratum pyramidale also appears increased (Fig. 6A and Supplementary Fig. 4). The cross-sectional areas of different hippocampal regions are unchanged in these aged mice suggesting the altered distribution and/or altered properties of the mutants do not impair neuron survival or induce significant neuronal atrophy (Supplementary Fig. 3). In contrast, Mossy fibers are tau positive in young mice, and there is no clear increase in tau staining in pyramidal neuron cell bodies. Instead, somatic staining of cells in the subgranular zone and some adjacent granule cells appears substantially increased in *Mapt*-9E18 mice, and to a lesser extent in *Mapt*-9A18 mice (Fig. 6B). In the cerebellum, reduced tau immunoreactivity is seen in the molecular layer of the cerebellar cortex in 24-month-old *Mapt*-9E18 mice, with a moderate reduction also apparent in *Mapt*-9A18 mice (Fig. 7A and B). Significant alterations to the ratio of tau immunoreactivity between the molecular layer and granule cell layer (Fig. 7B) most likely reflect a reduction in tau in the axons of granule cells (corresponding to the abundant parallel fibers in the molecular layer) relative to their soma.

Unfortunately, the cellular complexity of brain tissue largely precludes precise quantification of tau redistribution between different neuronal compartments due to frequent overlap of tau-positive axons and soma and/or dendrites of different neuron types in the same space. We therefore additionally assessed tau distribution in dissociated cultures of early postnatal cortical neurons and SCG neurons [a PNS neuron type that expresses a broad range of low molecular weight tau isoforms at this stage (Black et al., 1996)]. Whereas immunofluorescent staining revealed that distribution of the tau mutants appears relatively normal in cortical neuron cultures from both knockin lines (Supplementary Fig. 5), we found that 9E18tau distribution in *Mapt*-9E18 SCG neuron cultures differs strikingly from that of tau in wild-type cultures (Fig. 8A). Most notably, 9E18tau is relatively lacking in their long, axon-like neurites. Distribution of 9A18tau in *Mapt*-9A18 cultures, in contrast, appears relatively unaltered. 9E18tau also appears relatively increased in *Mapt*-9E18 SCG cell bodies using this method, but this is likely exaggerated by the low signal in surrounding neurites. We therefore performed an immunoblot analysis of ganglia (cell bodies and dendrites) and neurite ("axon") fractions from SCG explant cultures to accurately quantify the changes. This confirmed a relative paucity of 9E18tau in neurites (Fig. 8B) but also indicated that in SCG neurons, there is no reciprocal increase in 9E18tau in cell bodies and/or dendrites (Fig. 8B–D). Thus, whole-cell 9E18tau is reduced in SCGs, relative to wild-type tau in control cultures, consistent with reduced expression of 9E18tau in whole brain (Figs. 3–5 and Supplementary Fig. 2). Furthermore, and consistent with the immunofluorescence staining, immunoblotting confirmed that

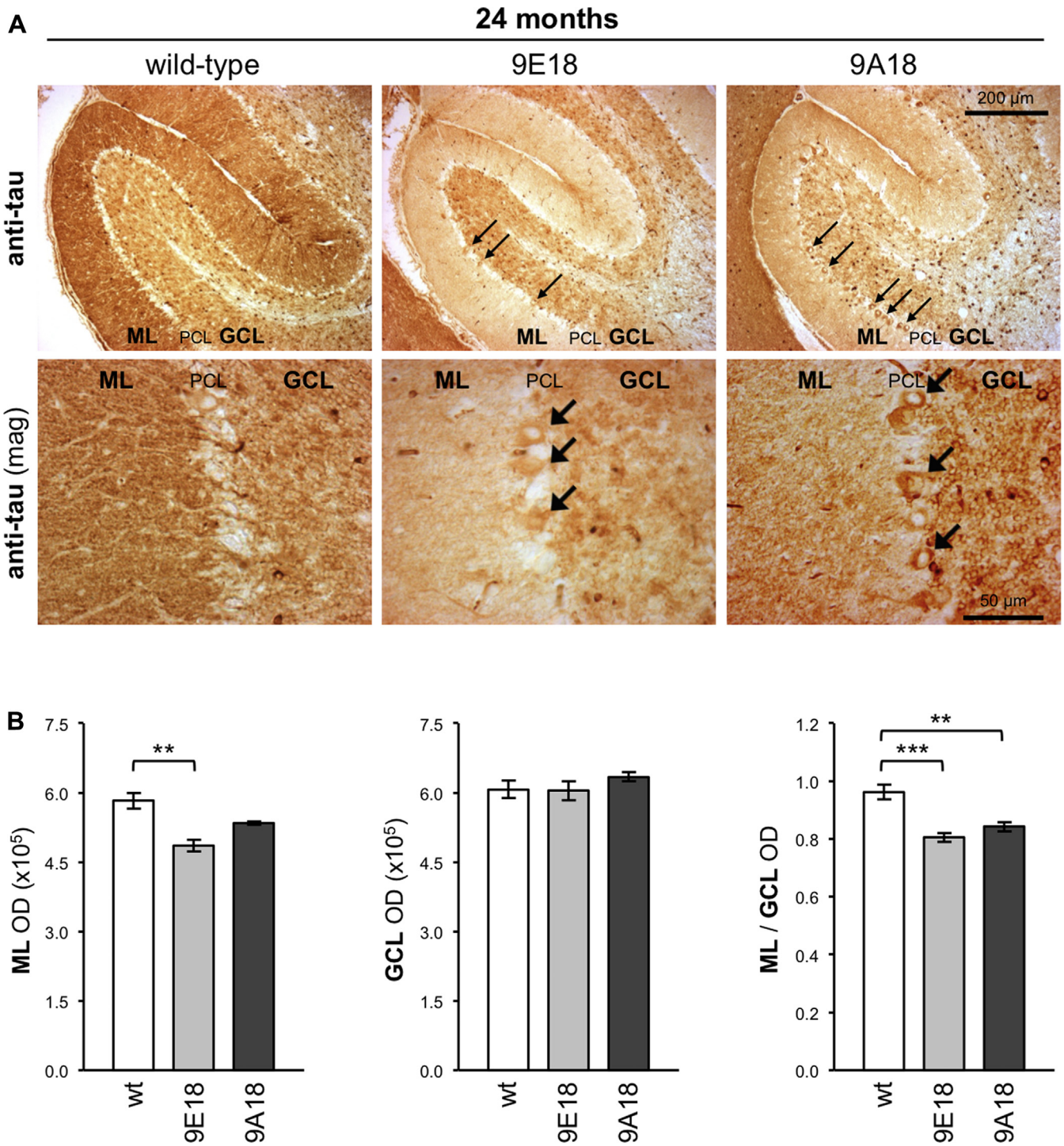

Fig. 7. Altered subcellular distribution of 9E18tau and 9A18tau in the cerebellum of knockin mice. (A) Representative immunohistochemical staining for total tau on brain tissue sections encompassing the molecular layer (ML), Purkinje cell layer (PCL), and granule cell layer (GCL) of the cerebellum from wild-type, *Mapt*-9E18, and *Mapt*-9A18 mice aged 24 months. Lower panels are at higher magnification. Parallel fibers (granule cell axons) in the molecular layer of the cerebellar cortex are strongly tau immunoreactive in wild-type mice, but this reactivity is visibly reduced in *Mapt*-9E18 mice, and to a lesser extent in *Mapt*-9A18 mice. Staining of Purkinje cell bodies in the Purkinje cell layer of both mutants also appears to be increased (arrows), but with some regional variation. Similar changes are seen in mice aged 21–26 months. Small, intensely stained cells present in sections of all genotypes, and particularly evident in the white matter, are tau-positive oligodendrocytes (Migheli et al., 1988). (B) Graphs showing the relative optical density (OD) of tau staining in the ML and GCL of the cerebellum, and the relative ML/GCL ratio, in *Mapt*-9E18 and *Mapt*-9A18 mice as a proportion of that in wild-type mice for mice aged 21–26 months (average 24 months). Means ± SEM are plotted for data from n = 3–5 animals per genotype. $^{**}p < 0.01$ and $^{***}p < 0.001$, one-way analysis of variance with Dunnett's multiple comparisons post hoc analysis. Abbreviation: SEM, standard error of the mean.

distribution of 9A18tau in these developmentally young neurons is essentially comparable to wild-type tau.

Together, these observations reveal consistent age-related changes in subcellular localization of both mutant tau proteins in some neuron types, with declines in axonal tau and accumulation of tau in soma and/or dendrites both being seen (although not necessarily simultaneously in the same neuron). However, there are also a few situations where only mislocalization of 9E18tau is seen,

or where 9E18tau mislocalization is clearly more pronounced. Interestingly, these differences are most apparent in neurons at earlier developmental stages.

3.7. *Mitochondrial flux is largely unaltered in* Mapt-*9E18 and* Mapt-*9A18 tibial nerve axons*

We previously identified changes in mitochondrial flux in tibial nerve axons of "P301L" tau knockin mice that we proposed may be linked to reduced microtubule binding and/or altered phosphorylation of the mutant tau (Gilley et al., 2012). We therefore assessed mitochondrial trafficking in tibial nerve axons from wild-type and *Mapt*-9E18 or *Mapt*-9A18 mice that were additionally heterozygous for the *Thy1-mitoCFP-S* (Mito-S) transgene (Misgeld et al., 2007). We found slight reductions in anterograde and retrograde flux of mitochondria in axons from both mutants aged between 5 and 9 months (although these changes did not reach statistical significance), and average and maximum speeds of the motile mitochondria were essentially unaltered (Supplementary Fig. 6). This contrasts with the increased flux of mitochondria observed in tibial nerve axons of "P301L" tau knockin mice at a similar age (Gilley et al., 2012).

4. Discussion

Our characterization of knockin mice exclusively expressing either phosphomimetic 9E18tau or phosphodefective 9A18tau

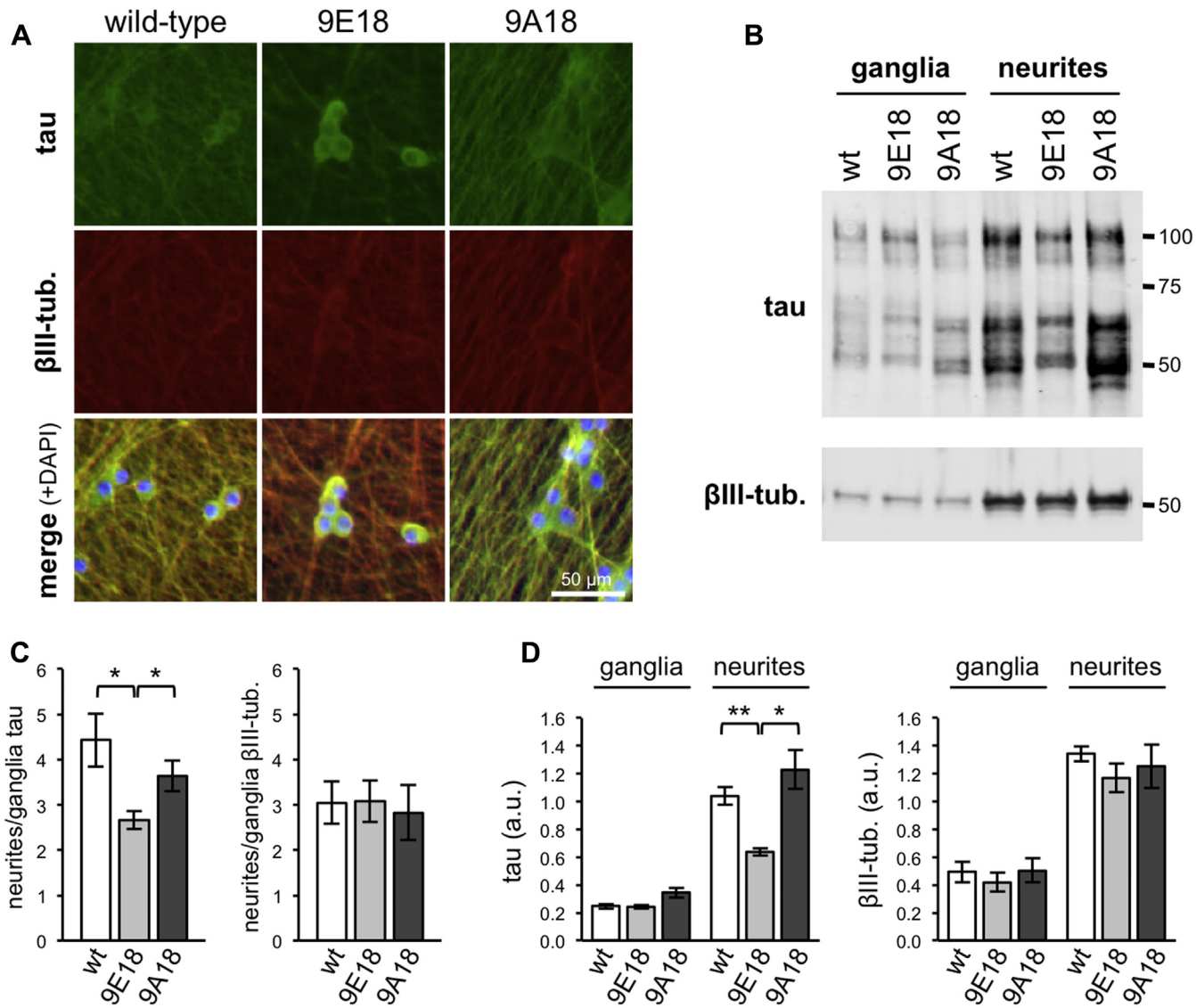

Fig. 8. Altered subcellular distribution of 9E18tau, but not 9A18tau, in primary *Mapt*-9E18 and *Mapt*-9A18 SCG neuronal cultures. (A) Representative images of immunofluorescent staining for total tau and βIII-tubulin (βIII-tub.) in dissociated SCG cultures from wild-type, *Mapt*-9E18, and *Mapt*-9A18 pups. Merge (+DAPI) images emphasize relative differences in tau and βIII-tubulin staining and show the location of counterstained cell bodies. (B) Representative immunoblot showing relative levels of total tau and βIII-tubulin in neurites and ganglia fractions from wild-type, *Mapt*-9E18, or *Mapt*-9A18 SCG explant cultures. Cultures are essentially devoid of non-neuronal cells, so separation of radial neurite outgrowth from their ganglia generates a neurite fraction highly enriched for axon-like processes and a ganglia fraction containing predominantly cell bodies and short dendrites (Gilley and Coleman, 2010; Peng et al., 1986). Slower migration of 9E18tau relative to wild-type tau is less evident in the SCG extracts compared to whole brains (see Fig. 1D and Fig. 4) likely due to high levels of natural, developmental tau phosphorylation in these cultured neurons taken from early postnatal pups. (C) Graphs showing relative proportions of tau and βIII-tubulin in neurite and ganglia fractions (neurite/ganglia ratios) and (D) graphs showing absolute total tau and βIII-tubulin levels in each fraction (a.u.=arbitrary units). Means ± SEM are plotted for data from n = 6 independent experiments. $^{*}p < 0.05$ and $^{**}p < 0.01$, repeated-measures one-way analysis of variance with Tukey's multiple comparisons post hoc analysis. Separate statistical tests were performed for ganglia and neurite fractions in (D). Abbreviation: SEM, standard error of the mean.

(without overexpression) has revealed several changes to tau function in vivo that are consistent with in vitro effects of altered tau phosphorylation. These include substantial reductions in the ability of 9E18tau to bind to and/or stabilize microtubules and to associate with membranes, with only modest or no changes seen for 9A18tau. Mislocalization of 9E18tau in some neuronal types also appears outwardly consistent with phosphorylation-dependent dissociation of tau from microtubules and relative redistribution from axons into the somatodendritic compartment, both of which have been proposed as critical early changes in the progression of tau pathology (Bancher et al., 1989; Braak et al., 1994; Mietelska-Porowska et al., 2014; Noble et al., 2013). However, we find that 9A18tau is also mislocalized in some of the same neuron types, especially in older mice, suggesting that 9E18tau mislocalization is at least partly independent of the pseudophosphorylation. Nevertheless, whatever the underlying cause, mislocalization of extensively pseudohyperphosphorylated 9E18tau does not appear to induce argyrophilic (Gallyas positive) inclusions, or even pretangle aggregation of tau, in mice up to at least 2 years of age. This result therefore questions whether tau hyperphosphorylation alone drives tau pathology, at least in mice.

The previous finding that pseudophosphorylation of just two of the mutated residues in 9E18tau, S202 and T205, is sufficient to promote filament formation in vitro (Rankin et al., 2005), makes the lack of advanced tau pathology in aged *Mapt*-9E18 mice somewhat surprising. One explanation may be that, because mice are relatively short-lived, downstream pathological changes may not have time to develop without localized or global overexpression of tau itself and/or its modulators (Gilley et al., 2011, 2012). There is also some debate about the relative propensities of murine and human tau to aggregate and form filaments. Notably, endogenous murine tau suppresses aggregation of wild-type or P301S mutant human tau in two mouse models (Ando et al., 2010, 2011; Andorfer et al., 2003), but there are also several situations where murine tau displays clear pathogenicity. These include its capacity to form filaments as efficiently as human tau in vitro (Chohan et al., 2005; Kampers et al., 1999), its ability to coaggregate with P301L mutant human tau in 3×Tg-AD transgenic mice and promote tangle pathology (Baglietto-Vargas et al., 2014), and the fact that pretangle and mature tau pathology can occur in the absence of human tau in some mouse models (Adams et al., 2009; Cruz et al., 2003; Liou et al., 2003). Because these models include p25 transgenic mice and *Pin1*$^{-/-}$ mice in which enhanced phosphorylation of endogenous murine tau alone seems to drive pathology (Cruz et al., 2003; Liou et al., 2003), it could be argued that the use of knockin mice in this study should not, in itself, preclude the appearance of tau pathology. Instead, a subset of mutations in 9E18tau could counteract the otherwise pathogenic effects of extensive pseudophosphorylation to account for the lack of late-stage tau pathology in *Mapt*-9E18 mice.

Although hyperphosphorylation of tau might generally favor aggregation (Iqbal et al., 2013), there is evidence that phosphorylation of some residues, including S214 and S262 (pseudophosphorylated in 9E18tau), can actually inhibit tau aggregation, even if the sites are subsequently phosphorylated once paired helical filaments have formed (Schneider et al., 1999). Studies in a *Drosophila* model also indicate there is some dissociation between tau phosphorylation and toxicity (Ambegaokar and Jackson, 2011; Chatterjee et al., 2009). Furthermore, although glutamate substitutions in 9E18tau do mimic phosphorylation in several respects, they may not fully replicate all aspects of this post-translational modification. Alternatively, these mutations could induce conformational changes that inhibit oligomerization or truncation of tau, both of which have been shown to promote assembly of tau into filaments (Lasagna-Reeves et al., 2012; Zilka et al., 2012).

The differential effect of the phosphomimetic and phosphodefective mutations on the relationship between tau and microtubules is also intriguing. A significant reduction in recovery of 9E18tau in brain microtubule fractions clearly infers a substantial effect of the glutamate substitutions on its capacity to bind microtubules, but, surprisingly, overall microtubule yield (based on βIII-tubulin recovery) is comparable to wild-type controls. One possible explanation is that the loss-of-function associated with 9E18tau might trigger compensatory changes during development to restore normal microtubule dynamics, similar to those proposed to occur in tau-deficient mice (Harada et al., 1994). Determining the nature of these changes could be revealing in terms of tau function and, although it has been suggested that MAP1A upregulation may compensate for a lack of tau during early development (Dawson et al., 2001; Fujio et al., 2007; Harada et al., 1994), it seems likely that there will be other critical changes that persist into adulthood. In contrast, a significantly reduced yield of microtubules from *Mapt*-9A18 brains (despite only a modest reduction in 9A18tau recovery, at best) would imply that the ability of 9A18tau to bind to and/or stabilize microtubules is also compromised in some way, but that this is not sufficient to trigger compensatory changes.

The substantial reduction in 9E18tau association with microtubules was perhaps predictable for two reasons. First, other pseudohyperphosphorylated tau mutants show a similar defect in vitro (Eidenmuller et al., 2001; Leger et al., 1997; Rodriguez-Martin et al., 2013; Smith et al., 2000) and second, the PRD, which normally interacts with the repeat domains to enhance this association (Brandt and Lee, 1993; Goode et al., 1997; Trinczek et al., 1995), is heavily modified in 9E18tau. However, the effects of combinatorial tau pseudophosphorylation at multiple sites are not easy to predict (Kiris et al., 2011), and it is notable that the extensively pseudophosphorylated human PHP tau does not appear to be defective for microtubule binding in cortical extracts (Hundelt et al., 2011). Only 5 of the 10 phosphomimetic mutations in human PHP tau match those in 9E18tau (S198E, S199E, S202E, T231E, and S235E), so reduced association of 9E18tau with microtubules can likely be attributed to one or more of its other 13 modifications. Significantly perhaps, this includes S262E in the first microtubule-binding repeat which alone has been shown to have a profound effect on the ability of tau to bind to and stabilize microtubules in vitro (Biernat et al., 1993; Drewes et al., 1995; Smith et al., 2000). In contrast, any potential reduction in the ability of 9A18tau to bind to and/or promote assembly of microtubules is at odds with enhanced microtubule association reported for the related, but distinct, phosphodefective human tau mutant, A18tau (Rodriguez-Martin et al., 2013). Although 9A18tau and human A18tau share 11 of 18 mutations, it is notable that two of the mutations unique to 9A18tau, S258A, and S262A are located within the first microtubule-binding repeat of tau. If either directly influences microtubule interactions in any way (unrelated to their inability to be phosphorylated), then it could account for any differences between the two phosphodefective mutants.

The correlation between the substantially reduced microtubule-binding capacity of 9E18tau and greatly reduced phosphorylation at the equivalent of human S396 in mouse tau is revealing because it supports our previous hypothesis, based on a similar correlation seen for “P301L” mutant tau, that defective microtubule binding reduces the need for nonpathological tau phosphorylation as a means to regulate microtubule dynamics (Gilley et al., 2012). Importantly, although the origin of the microtubule-binding defect is different for 9E18tau and “P301L” tau (pseudohyperphosphorylation vs. a disease-associated mutation), the outcome—reduced natural phosphorylation at S396—is the same. However, the significance of phosphorylation at this particular site is not clear; S396 pseudophosphorylation in human PHP tau does not alter

microtubule-binding in vivo (Hundelt et al., 2011), and it has only relatively modest effects on tau microtubule binding and/or microtubule assembly function in vitro (Ding et al., 2006; Smith et al., 2000). Therefore, rather than having a direct effect on tau binding to microtubules, S396 phosphorylation may instead be involved in the fine tuning of this interaction.

Given that membrane-associated tau has previously been shown to be largely dephosphorylated (Pooler et al., 2012), reduced membrane association of 9E18tau in *Mapt*-9E18 brain is also likely to be primarily a direct effect of its extensive pseudophosphorylation. This is further supported by the unaltered membrane association of 9A18tau in *Mapt*-9A18 brain. However, the large number of glutamate substitutions in 9E18tau, together with their limited overlap with other phosphomimetic mutants that show reduced membrane association (Eidenmuller et al., 2001; Pooler et al., 2012), precludes identification of specific sites that regulate this interaction. Modification of sites within or flanking PXXP motifs at residues 213-216 and/or 233-236 in the PRD domain of 9E18tau (human 2N4R tau numbering), including, but not restricted to T212E, S214E, T217E, T231E, S235E, and S237E, likely make some contribution as these motifs mediate phosphorylation-sensitive interaction of tau with membrane-associated SH3 domain-containing proteins, such as the protein tyrosine kinase FYN (Arrasate et al., 2000; Lee et al., 1998; Pooler et al., 2012; Reynolds et al., 2008). Overall (pseudo)phosphorylation load may also be important, given that pseudophosphorylation of other sites in the N-terminal half of tau can also independently inhibit tau association with membranes (Pooler et al., 2012). Of course, a contribution of pseudophosphorylation-independent effects, such as altered conformation induced specifically by the glutamate substitutions in 9E18tau, also cannot be ruled out.

The significant similarity in the mislocalization of 9E18tau and 9A18tau in neurons indicates that changes unrelated to their (pseudo)phosphorylation status are likely to be determinants of the phenotype, although pseudophosphorylation may still contribute to the seemingly more widespread and/or earlier mislocalization of 9E18tau. Several mechanisms have been proposed for subcellular sorting of tau (Zempel and Mandelkow, 2014), and common structural changes induced by both sets of mutations, perhaps specifically in relation to the conformation of the PRD, might interfere with any number of them. Disruption of two of the best characterized, a retrograde barrier in the axon initial segment that prevents tau re-entry into the soma (Li et al., 2011) and the preferential stabilization of tau in axons (Hirokawa et al., 1996), would be predicted to promote loss of tau from axons and/or its somatodendritic accumulation, similar to the mislocalization seen in both knockins. Both are also influenced by microtubule-binding capacity, thus providing another possible explanation for differences between the two mutants. An anterograde sorting mechanism could be an attractive alternative mechanism, but common suppression of anterograde trafficking of 9E18tau and 9A18tau seems unlikely given that the anterograde flow of other, partially related, phosphomimetic and phosphodefective tau mutants is differentially affected in primary rat cortical neurons (Cuchillo-Ibanez et al., 2008).

Whatever the mechanisms responsible for 9E18tau and 9A18tau mislocalization, variation in their efficacy in different neuron types or at different developmental stages could explain the apparent regional and temporal differences in mislocalization of the tau mutants. However, it is notable that reduced axonal levels of the mutants are most evident in vivo in neurons with unmyelinated, small caliber axons. Although it is possible that these neurons are the most susceptible to changes in tau homeostasis (Harada et al., 1994), the fact that their axons are also the most strongly tau immunoreactive raises the possibility that the phenotype is actually more widespread but simply cannot be visualized in other neuron types using standard immunohistochemistry techniques. Additional considerations include the possibility that reduced steady-state levels of 9E18tau, evident both in whole brain and SCG neuron cultures, make axonal deficiency of 9E18tau more perceptible than 9A18tau in some cases, or that some of the examples of mislocalization might instead reflect a developmental defect (e.g., in the subgranular zone of the dentate gyrus).

At present, the underlying basis for the counterintuitive differences in the steady-state levels of the mutant proteins and their mRNAs is not known. A possible reduction in 9E18tau stability in axons could perhaps account for the disparity between reduced steady-state levels of the protein and normal levels its mRNA in brain. However, in some contexts, phosphorylation has actually been shown to delay the proteasome-mediated turnover of tau via a mechanism that may involve Hsp90 (Dickey et al., 2007; Luo et al., 2007; Poppek et al., 2006; Rodriguez-Martin et al., 2013). Instead, reduced 9E18tau levels might reflect suboptimal translation, with the highly localized clustering of the substituting glutamate codons in *Mapt*-9E18 mRNA perhaps interfering with translational processivity. In contrast, changes at both the mRNA and protein levels are required to explain normal levels of 9A18tau protein in *Mapt*-9A18 brain when there is a simultaneous relative paucity of *Mapt*-9A18 mRNA. We speculate that transcription from the $Mapt^{9A18}$ knockin alleles could be impaired by exceptionally high GC-content in the targeted region (77% over 200 base pairs), although this would additionally require that 9A18tau is either more stable than wild-type tau, or is translated more efficiently, to account for normal expression of protein from a less-abundant mRNA pool.

Finally, we had also previously proposed a link between reduced microtubule-binding capacity and/or hypophosphorylation of "P301L" murine tau and the increased anterograde flux of mitochondria in tibial nerve axons in relatively young "P301L" murine tau knockin mice (Gilley et al., 2012). The absence of similar effects on mitochondrial trafficking in *Mapt*-9E18 tibial nerve axons, despite 9E18tau showing seemingly more pronounced changes to these properties, seems to rule out their involvement in increasing anterograde transport. However, compensatory changes (as discussed previously) could mask similar effects if they are triggered during development in response to the severe dysfunction associated with 9E18tau, but not the more moderate dysfunction of "P301L" murine tau (Gilley et al., 2012). Notably, both the yield and tau/tubulin ratio of microtubules appear to be reduced in knockin mice exclusively expressing "P301L" tau (Gilley et al., 2012). This differentiates these mice from both *Mapt*-9E18 and *Mapt*-9A18 mice where just one or other, but not both, are altered and could explain why only "P301L" murine tau knockin mice display alterations in mitochondrial trafficking.

To conclude, our characterization of complementary *Mapt*-9E18 and *Mapt*-9A18 phosphomimetic and phosphodefective tau knockin mice provides important new insight into the potential impact of phosphorylation of the PRD and neighboring first MTBD on a number of key properties of tau when expressed at near-physiological levels in vivo. Crucially, the findings also raise a number of important questions about the role of tau hyperphosphorylation in the pathogenesis of human tauopathies. These questions can be addressed in future studies of other phosphomimetic and phosphodefective tau animal models.

Disclosure statement

The authors declare there are no actual or potential conflicts of interest relating to this work. All animal work in this study was performed following UK Home Office guidelines after the project

had been approved following an appropriate ethical review process at the Babraham Institute.

Acknowledgements

The authors thank the Babraham Institute Gene Targeting Facility, and Dr. Anne Segonds-Pichon for statistical help. This work was supported by the UK Medical Research Council (G0300408) an Institute Strategic Programme Grant from the UK Biotechnology and Biological Sciences Research Council, the Henry Smith Charity, Alzheimer's Research UK (ART/EG2004A/1, ART-TRF2011-2), the Wellcome Trust (WT088033MA), the Belgian Fonds de la Recherche Scientifique Médicale (T.0023.15), the Belgian Foundation for Alzheimer Research (FRA/SAO, S#14001) and Fund Aline (King Baudoin Foundation), the IAP program (P7/16) of the Belgian Federal Science Policy Office, and the Belgian Fonds National de la Recherche Scientifique.

Appendix A. Supplementary data

Supplementary data associated with this article can be found, in the online version, at http://dx.doi.org/10.1016/j.neurobiolaging.2015.11.028.

References

Adams, S.J., Crook, R.J., Deture, M., Randle, S.J., Innes, A.E., Yu, X.Z., Lin, W.L., Dugger, B.N., McBride, M., Hutton, M., Dickson, D.W., McGowan, E., 2009. Overexpression of wild-type murine tau results in progressive tauopathy and neurodegeneration. Am. J. Pathol. 175, 1598–1609.

Ahlijanian, M.K., Barrezueta, N.X., Williams, R.D., Jakowski, A., Kowsz, K.P., McCarthy, S., Coskran, T., Carlo, A., Seymour, P.A., Burkhardt, J.E., Nelson, R.B., McNeish, J.D., 2000. Hyperphosphorylated tau and neurofilament and cytoskeletal disruptions in mice overexpressing human p25, an activator of cdk5. Proc. Natl. Acad. Sci. U. S. A. 97, 2910–2915.

Ambegaokar, S.S., Jackson, G.R., 2011. Functional genomic screen and network analysis reveal novel modifiers of tauopathy dissociated from tau phosphorylation. Hum. Mol. Genet. 20, 4947–4977.

Ando, K., Leroy, K., Heraud, C., Kabova, A., Yilmaz, Z., Authelet, M., Suain, V., De Decker, R., Brion, J.P., 2010. Deletion of murine tau gene increases tau aggregation in a human mutant tau transgenic mouse model. Biochem. Soc. Trans. 38, 1001–1005.

Ando, K., Leroy, K., Heraud, C., Yilmaz, Z., Authelet, M., Suain, V., De Decker, R., Brion, J.P., 2011. Accelerated human mutant tau aggregation by knocking out murine tau in a transgenic mouse model. Am. J. Pathol. 178, 803–816.

Andorfer, C., Kress, Y., Espinoza, M., de Silva, R., Tucker, K.L., Barde, Y.A., Duff, K., Davies, P., 2003. Hyperphosphorylation and aggregation of tau in mice expressing normal human tau isoforms. J. Neurochem. 86, 582–590.

Andreadis, A., Brown, W.M., Kosik, K.S., 1992. Structure and novel exons of the human tau gene. Biochemistry 31, 10626–10633.

Andrews, S., Gilley, J., Coleman, M.P., 2010. Difference Tracker: ImageJ plugins for fully automated analysis of multiple axonal transport parameters. J. Neurosci. Methods 193, 281–287.

Arrasate, M., Perez, M., Avila, J., 2000. Tau dephosphorylation at tau-1 site correlates with its association to cell membrane. Neurochem. Res. 25, 43–50.

Baglietto-Vargas, D., Kitazawa, M., Le, E.J., Estrada-Hernandez, T., Rodriguez-Ortiz, C.J., Medeiros, R., Green, K.N., LaFerla, F.M., 2014. Endogenous murine tau promotes neurofibrillary tangles in 3xTg-AD mice without affecting cognition. Neurobiol. Dis. 62, 407–415.

Bancher, C., Brunner, C., Lassmann, H., Budka, H., Jellinger, K., Wiche, G., Seitelberger, F., Grundke-Iqbal, I., Iqbal, K., Wisniewski, H.M., 1989. Accumulation of abnormally phosphorylated tau precedes the formation of neurofibrillary tangles in Alzheimer's disease. Brain Res. 477, 90–99.

Biernat, J., Gustke, N., Drewes, G., Mandelkow, E.M., Mandelkow, E., 1993. Phosphorylation of Ser262 strongly reduces binding of tau to microtubules: distinction between PHF-like immunoreactivity and microtubule binding. Neuron 11, 153–163.

Black, M.M., Slaughter, T., Moshiach, S., Obrocka, M., Fischer, I., 1996. Tau is enriched on dynamic microtubules in the distal region of growing axons. J. Neurosci. 16, 3601–3619.

Braak, E., Braak, H., Mandelkow, E.M., 1994. A sequence of cytoskeleton changes related to the formation of neurofibrillary tangles and neuropil threads. Acta Neuropathol. 87, 554–567.

Bramblett, G.T., Goedert, M., Jakes, R., Merrick, S.E., Trojanowski, J.Q., Lee, V.M., 1993. Abnormal tau phosphorylation at Ser396 in Alzheimer's disease recapitulates development and contributes to reduced microtubule binding. Neuron 10, 1089–1099.

Bramblett, G.T., Trojanowski, J.Q., Lee, V.M., 1992. Regions with abundant neurofibrillary pathology in human brain exhibit a selective reduction in levels of binding-competent tau and accumulation of abnormal tau-isoforms (A68 proteins). Lab. Invest. 66, 212–222.

Brandt, R., Lee, G., 1993. Functional organization of microtubule-associated protein tau. Identification of regions which affect microtubule growth, nucleation, and bundle formation in vitro. J. Biol. Chem. 268, 3414–3419.

Brandt, R., Leger, J., Lee, G., 1995. Interaction of tau with the neural plasma membrane mediated by tau's amino-terminal projection domain. J. Cell Biol. 131, 1327–1340.

Brion, J.P., Hanger, D.P., Bruce, M.T., Couck, A.M., Flament-Durand, J., Anderton, B.H., 1991. Tau in Alzheimer neurofibrillary tangles. N- and C-terminal regions are differentially associated with paired helical filaments and the location of a putative abnormal phosphorylation site. Biochem. J. 273 (Pt 1), 127–133.

Brion, J.P., Smith, C., Couck, A.M., Gallo, J.M., Anderton, B.H., 1993. Developmental changes in tau phosphorylation: fetal tau is transiently phosphorylated in a manner similar to paired helical filament-tau characteristic of Alzheimer's disease. J. Neurochem. 61, 2071–2080.

Busciglio, J., Lorenzo, A., Yeh, J., Yankner, B.A., 1995. beta-amyloid fibrils induce tau phosphorylation and loss of microtubule binding. Neuron 14, 879–888.

Chatterjee, S., Sang, T.K., Lawless, G.M., Jackson, G.R., 2009. Dissociation of tau toxicity and phosphorylation: role of GSK-3beta, MARK and Cdk5 in a Drosophila model. Hum. Mol. Genet. 18, 164–177.

Chohan, M.O., Haque, N., Alonso, A., El-Akkad, E., Grundke-Iqbal, I., Grover, A., Iqbal, K., 2005. Hyperphosphorylation-induced self assembly of murine tau: a comparison with human tau. J. Neural Transm. 112, 1035–1047.

Cruz, J.C., Tseng, H.C., Goldman, J.A., Shih, H., Tsai, L.H., 2003. Aberrant Cdk5 activation by p25 triggers pathological events leading to neurodegeneration and neurofibrillary tangles. Neuron 40, 471–483.

Cuchillo-Ibanez, I., Seereeram, A., Byers, H.L., Leung, K.Y., Ward, M.A., Anderton, B.H., Hanger, D.P., 2008. Phosphorylation of tau regulates its axonal transport by controlling its binding to kinesin. FASEB J. 22, 3186–3195.

Davis, D.R., Brion, J.P., Couck, A.M., Gallo, J.M., Hanger, D.P., Ladhani, K., Lewis, C., Miller, C.C., Rupniak, T., Smith, C., Anderton, B.H., 1995. The phosphorylation state of the microtubule-associated protein tau as affected by glutamate, colchicine and beta-amyloid in primary rat cortical neuronal cultures. Biochem. J. 309 (Pt 3), 941–949.

Dawson, H.N., Ferreira, A., Eyster, M.V., Ghoshal, N., Binder, L.I., Vitek, M.P., 2001. Inhibition of neuronal maturation in primary hippocampal neurons from tau deficient mice. J. Cell Sci. 114 (Pt 6), 1179–1187.

Denk, F., Wade-Martins, R., 2009. Knock-out and transgenic mouse models of tauopathies. Neurobiol. Aging 30, 1–13.

Dickey, C.A., Kamal, A., Lundgren, K., Klosak, N., Bailey, R.M., Dunmore, J., Ash, P., Shoraka, S., Zlatkovic, J., Eckman, C.B., Patterson, C., Dickson, D.W., Nahman Jr., N.S., Hutton, M., Burrows, F., Petrucelli, L., 2007. The high-affinity HSP90-CHIP complex recognizes and selectively degrades phosphorylated tau client proteins. J. Clin. Invest. 117, 648–658.

Ding, H., Matthews, T.A., Johnson, G.V., 2006. Site-specific phosphorylation and caspase cleavage differentially impact tau-microtubule interactions and tau aggregation. J. Biol. Chem. 281, 19107–19114.

Drewes, G., Trinczek, B., Illenberger, S., Biernat, J., Schmitt-Ulms, G., Meyer, H.E., Mandelkow, E.M., Mandelkow, E., 1995. Microtubule-associated protein/microtubule affinity-regulating kinase (p110mark). A novel protein kinase that regulates tau-microtubule interactions and dynamic instability by phosphorylation at the Alzheimer-specific site serine 262. J. Biol. Chem. 270, 7679–7688.

Eidenmuller, J., Fath, T., Maas, T., Pool, M., Sontag, E., Brandt, R., 2001. Phosphorylation-mimicking glutamate clusters in the proline-rich region are sufficient to simulate the functional deficiencies of hyperphosphorylated tau protein. Biochem. J. 357 (Pt 3), 759–767.

Fujio, K., Sato, M., Uemura, T., Sato, T., Sato-Harada, R., Harada, A., 2007. 14-3-3 proteins and protein phosphatases are not reduced in tau-deficient mice. Neuroreport 18, 1049–1052.

Gilley, J., Adalbert, R., Coleman, M.P., 2011. Modelling early responses to neurodegenerative mutations in mice. Biochem. Soc. Trans. 39, 933–938.

Gilley, J., Adalbert, R., Yu, G., Coleman, M.P., 2013. Rescue of peripheral and CNS axon defects in mice lacking NMNAT2. J. Neurosci. 33, 13410–13424.

Gilley, J., Coleman, M.P., 2010. Endogenous Nmnat2 is an essential survival factor for maintenance of healthy axons. PLoS Biol. 8, e1000300.

Gilley, J., Seereeram, A., Ando, K., Mosely, S., Andrews, S., Kerschensteiner, M., Misgeld, T., Brion, J.P., Anderton, B., Hanger, D.P., Coleman, M.P., 2012. Age-dependent axonal transport and locomotor changes and tau hypophosphorylation in a "P301L" tau knockin mouse. Neurobiol. Aging 33, 621.e1–621.e15.

Goode, B.L., Denis, P.E., Panda, D., Radeke, M.J., Miller, H.P., Wilson, L., Feinstein, S.C., 1997. Functional interactions between the proline-rich and repeat regions of tau enhance microtubule binding and assembly. Mol. Biol. Cell 8, 353–365.

Hanger, D.P., Anderton, B.H., Noble, W., 2009. Tau phosphorylation: the therapeutic challenge for neurodegenerative disease. Trends Mol. Med. 15, 112–119.

Hanger, D.P., Betts, J.C., Loviny, T.L., Blackstock, W.P., Anderton, B.H., 1998. New phosphorylation sites identified in hyperphosphorylated tau (paired helical filament-tau) from Alzheimer's disease brain using nanoelectrospray mass spectrometry. J. Neurochem. 71, 2465–2476.

Hanger, D.P., Byers, H.L., Wray, S., Leung, K.Y., Saxton, M.J., Seereeram, A., Reynolds, C.H., Ward, M.A., Anderton, B.H., 2007. Novel phosphorylation sites in tau from Alzheimer brain support a role for casein kinase 1 in disease pathogenesis. J. Biol. Chem. 282, 23645–23654.

Harada, A., Oguchi, K., Okabe, S., Kuno, J., Terada, S., Ohshima, T., Sato-Yoshitake, R., Takei, Y., Noda, T., Hirokawa, N., 1994. Altered microtubule organization in small-calibre axons of mice lacking tau protein. Nature 369, 488–491.

Hirokawa, N., Funakoshi, T., Sato-Harada, R., Kanai, Y., 1996. Selective stabilization of tau in axons and microtubule-associated protein 2C in cell bodies and dendrites contributes to polarized localization of cytoskeletal proteins in mature neurons. J. Cell Biol. 132, 667–679.

Hundelt, M., Fath, T., Selle, K., Oesterwind, K., Jordan, J., Schultz, C., Gotz, J., von Engelhardt, J., Monyer, H., Lewejohann, L., Sachser, N., Bakota, L., Brandt, R., 2011. Altered phosphorylation but no neurodegeneration in a mouse model of tau hyperphosphorylation. Neurobiol. Aging 32, 991–1006.

Iqbal, K., Gong, C.X., Liu, F., 2013. Hyperphosphorylation-induced tau oligomers. Front. Neurol. 4, 112.

Ittner, L.M., Gotz, J., 2011. Amyloid-beta and tau–a toxic pas de deux in Alzheimer's disease. Nat. Rev. Neurosci. 12, 65–72.

Johnson, G.V., Stoothoff, W.H., 2004. Tau phosphorylation in neuronal cell function and dysfunction. J. Cell Sci. 117 (Pt 24), 5721–5729.

Kampers, T., Pangalos, M., Geerts, H., Wiech, H., Mandelkow, E., 1999. Assembly of paired helical filaments from mouse tau: implications for the neurofibrillary pathology in transgenic mouse models for Alzheimer's disease. FEBS Lett. 451, 39–44.

Kanai, Y., Takemura, R., Oshima, T., Mori, H., Ihara, Y., Yanagisawa, M., Masaki, T., Hirokawa, N., 1989. Expression of multiple tau isoforms and microtubule bundle formation in fibroblasts transfected with a single tau cDNA. J. Cell Biol. 109, 1173–1184.

Kiris, E., Ventimiglia, D., Sargin, M.E., Gaylord, M.R., Altinok, A., Rose, K., Manjunath, B.S., Jordan, M.A., Wilson, L., Feinstein, S.C., 2011. Combinatorial Tau pseudophosphorylation: markedly different regulatory effects on microtubule assembly and dynamic instability than the sum of the individual parts. J. Biol. Chem. 286, 14257–14270.

Kolarova, M., Garcia-Sierra, F., Bartos, A., Ricny, J., Ripova, D., 2012. Structure and pathology of tau protein in Alzheimer disease. Int. J. Alzheimers Dis. 2012, 731526.

Kopke, E., Tung, Y.C., Shaikh, S., Alonso, A.C., Iqbal, K., Grundke-Iqbal, I., 1993. Microtubule-associated protein tau. Abnormal phosphorylation of a non-paired helical filament pool in Alzheimer disease. J. Biol. Chem. 268, 24374–24384.

Ksiezak-Reding, H., Liu, W.K., Yen, S.H., 1992. Phosphate analysis and dephosphorylation of modified tau associated with paired helical filaments. Brain Res. 597, 209–219.

Lasagna-Reeves, C.A., Castillo-Carranza, D.L., Sengupta, U., Sarmiento, J., Troncoso, J., Jackson, G.R., Kayed, R., 2012. Identification of oligomers at early stages of tau aggregation in Alzheimer's disease. FASEB J. 26, 1946–1959.

Lee, G., Newman, S.T., Gard, D.L., Band, H., Panchamoorthy, G., 1998. Tau interacts with src-family non-receptor tyrosine kinases. J. Cell Sci. 111 (Pt 21), 3167–3177.

Leger, J., Kempf, M., Lee, G., Brandt, R., 1997. Conversion of serine to aspartate imitates phosphorylation-induced changes in the structure and function of microtubule-associated protein tau. J. Biol. Chem. 272, 8441–8446.

Leroy, K., Bretteville, A., Schindowski, K., Gilissen, E., Authelet, M., De Decker, R., Yilmaz, Z., Buee, L., Brion, J.P., 2007. Early axonopathy preceding neurofibrillary tangles in mutant tau transgenic mice. Am. J. Pathol. 171, 976–992.

Li, X., Kumar, Y., Zempel, H., Mandelkow, E.M., Biernat, J., Mandelkow, E., 2011. Novel diffusion barrier for axonal retention of Tau in neurons and its failure in neurodegeneration. EMBO J. 30, 4825–4837.

Liou, Y.C., Sun, A., Ryo, A., Zhou, X.Z., Yu, Z.X., Huang, H.K., Uchida, T., Bronson, R., Bing, G., Li, X., Hunter, T., Lu, K.P., 2003. Role of the prolyl isomerase Pin1 in protecting against age-dependent neurodegeneration. Nature 424, 556–561.

Luo, W., Dou, F., Rodina, A., Chip, S., Kim, J., Zhao, Q., Moulick, K., Aguirre, J., Wu, N., Greengard, P., Chiosis, G., 2007. Roles of heat-shock protein 90 in maintaining and facilitating the neurodegenerative phenotype in tauopathies. Proc. Natl. Acad. Sci. U. S. A. 104, 9511–9516.

Maas, T., Eidenmuller, J., Brandt, R., 2000. Interaction of tau with the neural membrane cortex is regulated by phosphorylation at sites that are modified in paired helical filaments. J. Biol. Chem. 275, 15733–15740.

Mietelska-Porowska, A., Wasik, U., Goras, M., Filipek, A., Niewiadomska, G., 2014. Tau protein modifications and interactions: their role in function and dysfunction. Int. J. Mol. Sci. 15, 4671–4713.

Migheli, A., Butler, M., Brown, K., Shelanski, M.L., 1988. Light and electron microscope localization of the microtubule-associated tau protein in rat brain. J. Neurosci. 8, 1846–1851.

Misgeld, T., Kerschensteiner, M., Bareyre, F.M., Burgess, R.W., Lichtman, J.W., 2007. Imaging axonal transport of mitochondria in vivo. Nat. Methods 4, 559–561.

Morris, M., Knudsen, G.M., Maeda, S., Trinidad, J.C., Ioanoviciu, A., Burlingame, A.L., Mucke, L., 2015. Tau post-translational modifications in wild-type and human amyloid precursor protein transgenic mice. Nat. Neurosci. 18, 1183–1189.

Noble, W., Hanger, D.P., Gallo, J.M., 2010. Transgenic mouse models of tauopathy in drug discovery. CNS Neurol. Disord. Drug Targets 9, 403–428.

Noble, W., Hanger, D.P., Miller, C.C., Lovestone, S., 2013. The importance of tau phosphorylation for neurodegenerative diseases. Front. Neurol. 4, 83.

Noble, W., Olm, V., Takata, K., Casey, E., Mary, O., Meyerson, J., Gaynor, K., LaFrancois, J., Wang, L., Kondo, T., Davies, P., Burns, M., Veeranna, Nixon, R., Dickson, D., Matsuoka, Y., Ahlijanian, M., Lau, L.F., Duff, K., 2003. Cdk5 is a key factor in tau aggregation and tangle formation in vivo. Neuron 38, 555–565.

Peng, I., Binder, L.I., Black, M.M., 1986. Biochemical and immunological analyses of cytoskeletal domains of neurons. J. Cell Biol. 102, 252–262.

Pooler, A.M., Usardi, A., Evans, C.J., Philpott, K.L., Noble, W., Hanger, D.P., 2012. Dynamic association of tau with neuronal membranes is regulated by phosphorylation. Neurobiol. Aging 33, 431.e27–431.e38.

Poppek, D., Keck, S., Ermak, G., Jung, T., Stolzing, A., Ullrich, O., Davies, K.J., Grune, T., 2006. Phosphorylation inhibits turnover of the tau protein by the proteasome: influence of RCAN1 and oxidative stress. Biochem. J. 400, 511–520.

Rankin, C.A., Sun, Q., Gamblin, T.C., 2005. Pseudo-phosphorylation of tau at Ser202 and Thr205 affects tau filament formation. Brain Res. Mol. Brain Res. 138, 84–93.

Reynolds, C.H., Garwood, C.J., Wray, S., Price, C., Kellie, S., Perera, T., Zvelebil, M., Yang, A., Sheppard, P.W., Varndell, I.M., Hanger, D.P., Anderton, B.H., 2008. Phosphorylation regulates tau interactions with Src homology 3 domains of phosphatidylinositol 3-kinase, phospholipase Cgamma1, Grb2, and Src family kinases. J. Biol. Chem. 283, 18177–18186.

Rodriguez-Martin, T., Cuchillo-Ibanez, I., Noble, W., Nyenya, F., Anderton, B.H., Hanger, D.P., 2013. Tau phosphorylation affects its axonal transport and degradation. Neurobiol. Aging 34, 2146–2157.

Schneider, A., Biernat, J., von Bergen, M., Mandelkow, E., Mandelkow, E.M., 1999. Phosphorylation that detaches tau protein from microtubules (Ser262, Ser214) also protects it against aggregation into Alzheimer paired helical filaments. Biochemistry 38, 3549–3558.

Smith, M.J., Crowther, R.A., Goedert, M., 2000. The natural osmolyte trimethylamine N-oxide (TMAO) restores the ability of mutant tau to promote microtubule assembly. FEBS Lett. 484, 265–270.

Spittaels, K., Van den Haute, C., Van Dorpe, J., Geerts, H., Mercken, M., Bruynseels, K., Lasrado, R., Vandezande, K., Laenen, I., Boon, T., Van Lint, J., Vandenheede, J., Moechars, D., Loos, R., Van Leuven, F., 2000. Glycogen synthase kinase-3beta phosphorylates protein tau and rescues the axonopathy in the central nervous system of human four-repeat tau transgenic mice. J. Biol. Chem. 275, 41340–41349.

Takuma, H., Arawaka, S., Mori, H., 2003. Isoforms changes of tau protein during development in various species. Brain Res. Dev. Brain Res. 142, 121–127.

Terwel, D., Muyllaert, D., Dewachter, I., Borghgraef, P., Croes, S., Devijver, H., Van Leuven, F., 2008. Amyloid activates GSK-3beta to aggravate neuronal tauopathy in bigenic mice. Am. J. Pathol. 172, 786–798.

Trinczek, B., Biernat, J., Baumann, K., Mandelkow, E.M., Mandelkow, E., 1995. Domains of tau protein, differential phosphorylation, and dynamic instability of microtubules. Mol. Biol. Cell. 6, 1887–1902.

Wagner, U., Utton, M., Gallo, J.M., Miller, C.C., 1996. Cellular phosphorylation of tau by GSK-3 beta influences tau binding to microtubules and microtubule organisation. J. Cell Sci. 109 (Pt 6), 1537–1543.

Wolfe, M.S., 2009. Tau mutations in neurodegenerative diseases. J. Biol. Chem. 284, 6021–6025.

Zempel, H., Mandelkow, E., 2014. Lost after translation: missorting of Tau protein and consequences for Alzheimer disease. Trends Neurosci. 37, 721–732.

Zilka, N., Kovacech, B., Barath, P., Kontsekova, E., Novak, M., 2012. The self-perpetuating tau truncation circle. Biochem. Soc. Trans. 40, 681–686.